Wnt signalling, cell fate determination and anteroposterior polarity of the skate gill arch skeleton

Jenaid M. Rees[1], Victoria A. Sleight[2], Stephen J. Clark[3], Tetsuya Nakamura[4] and J. Andrew Gillis[1,5,*]

[1]Department of Zoology, University of Cambridge, Cambridge CB2 3EJ, United Kingdom

[2]School of Biological sciences, University of Aberdeen, Aberdeen, AB24 3FX

[3]Babraham Institute, Cambridge, United Kingdom

[4]Department of Genetics, Rutgers University

[5]Marine Biological Laboratory, Woods Hole, MA, 02543

*Correspondence: jag93@cam.ac.uk

The gill arch skeleton of cartilaginous fishes (sharks, skates, rays and holocephalans) exhibits anterior–posterior polarity, with a series of appendages (branchial rays) projecting from the posterior margin of the gill arch cartilages. We previously demonstrated in the skate (*Leucoraja erinacea*) that branchial rays derive from a posterior domain of pharyngeal arch mesenchyme, which is responsive to Shh signalling from a distal gill arch epithelial ridge (GAER) signalling centre. However, how branchial ray progenitors are specified exclusively within posterior gill arch mesenchyme is not known. Here we show that the GAER of the skate is of endodermal origin, arises at the endoderm–ectoderm boundary, and is a source of Fgf and Shh signals that are transduced broadly and posteriorly, respectively, within underlying arch mesenchyme. Using RNAseq, we discover that genes encoding several Wnt ligands are expressed in the ectoderm immediately adjacent to the GAER, and that these Wnt signals are transduced largely in the anterior arch mesenchyme. These tissue origin and gene expression features are largely conserved in the hyoid arch of the chick and are therefore likely an ancestral feature of jawed vertebrates. Finally, using pharmacological manipulations in skate, we show that loss of Wnt signalling results in an anterior expansion of Shh signal transduction within pharyngeal arch epithelium, and the formation of ectopic anterior branchial rays. Our findings demonstrate that Wnt signalling restricts chondrogenesis to the posterior gill arch and highlights the importance of signalling interactions at embryonic tissue boundaries for cell fate determination in pharyngeal arches.

Introduction

The pharyngeal arches of vertebrate embryos give rise to much of the craniofacial skeleton, including the skeleton of the jaws and gills in fishes, and of the jaw, auditory ossicles and larynx in amniotes (Graham and Smith, 2001). The arches are formed through iterative outpockets of foregut endoderm that contact the overlying surface ectoderm. The meeting of endoderm and ectoderm generates a series of columns lined laterally by ectoderm, medially by endoderm, and containing a core of mesoderm and neural crest-derived mesenchyme (Graham and Smith, 2001). In fishes, endodermal outpockets fuse with the overlying surface ectoderm, giving rise to the gill slits and the respiratory surfaces of the gill arches (Gillis and Tidswell, 2017). In amniotes, the endodermal outpockets give rise to glandular tissues, such as the tonsils, parathyroid and ultimobranchial glands (Grevellec and Tucker, 2010). In all vertebrates, the largely neural crest-derived mesenchyme of the pharyngeal arches gives rise to the pharyngeal skeleton (Jiang et al., 2002, Kague et al., 2012, Sleight and Gillis, 2020, Couly and Le Douarin, 1990), and receives patterning and polarity information via signals from adjacent epithelia (Veitch et al., 1999, Gillis et al., 2009b, Couly et al., 2002, Brito et al., 2006).

All jawed vertebrates belong to one of two lineages: cartilaginous fishes (sharks, skates, rays and holocephalans) or bony fishes (ray- and lobe-fined fishes, the latter including tetrapods). While the gill arch skeleton of both cartilaginous and bony fishes ancestrally consisted proximally of two principal gill arch cartilages (the epi- and ceratobranchials), the gill arch skeleton of cartilaginous fishes additionally includes a distal series of fine cartilaginous rods called branchial rays (Fig.1A,B). These rays reflect the clear anteroposterior polarity of the gill arch skeleton of cartilaginous fishes, originating along the posterior margin of the epi- and ceratobranchial cartilages, and projecting laterally into the interbranchial septum of each arch (Gillis et al., 2009a). Elasmobranch cartilaginous fishes (sharks, skates and rays) possess five sets of branchial rays, associated with their hyoid (2nd pharyngeal) and first four gill arches. Holocephalans, on the other hand, possess a single set of branchial rays supporting their hyoid arch-derived operculum.

The branchial rays of cartilaginous fishes develop under the influence of the gill arch epithelial ridge (GAER): a *sonic hedgehog* (*Shh*)-expressing signalling centre located within the posterior-distal epithelium of the gill arches (Fig.1C,D) (Gillis et al., 2009b). As the gill arches undergo a prolonged phase of lateral expansion, Shh signalling from the GAER is asymmetrically transduced within the posterior arch environment, as evidenced by posterior expression of *Ptc2* in gill arch mesenchyme and epithelium. This posterior transduction of Shh signalling, in turn, appears to underlie the anteroposterior polarity of the gill arch skeleton, as branchial rays derive exclusively from posterior–distal (Shh-responsive/GAER-adjacent) gill arch mesenchyme (Gillis and Hall, 2016). In the skate, application of exogenous Shh protein within gill arches is sufficient to induce ectopic branchial ray formation, and targeted or systemic inhibition of hedgehog signalling using cyclopamine results in branchial ray deletion (Gillis et al., 2009b). However, whether other signalling mechanisms function alongside or in conjunction with GAER Shh signalling to establish and maintain gill arch skeletal polarity remains unexplored.

Here, we show that the GAER of the little skate (*Leucoraja erinacea*) is of endodermal origin and arises at the endoderm–ectoderm interface of each pharyngeal arch. We find that the ectoderm immediately adjacent to the GAER expresses several genes encoding Wnt ligands and that these Wnt signals are transduced in the anterior arch environment in a pattern that is broadly complementary to the posterior transduction of GAER Shh signalling. Finally, inhibition Wnt signalling in developing skate embryos results in an anterior expansion of Shh signalling transduction, and in the formation of ectopic branchial rays in the anterior gill arch. We propose that Wnt signalling from pharyngeal arch ectoderm contributes to maintenance of anterior–posterior polarity of the skate gill arch skeleton by repressing Shh signalling and chondrogenesis to the posterior gill arch territory.

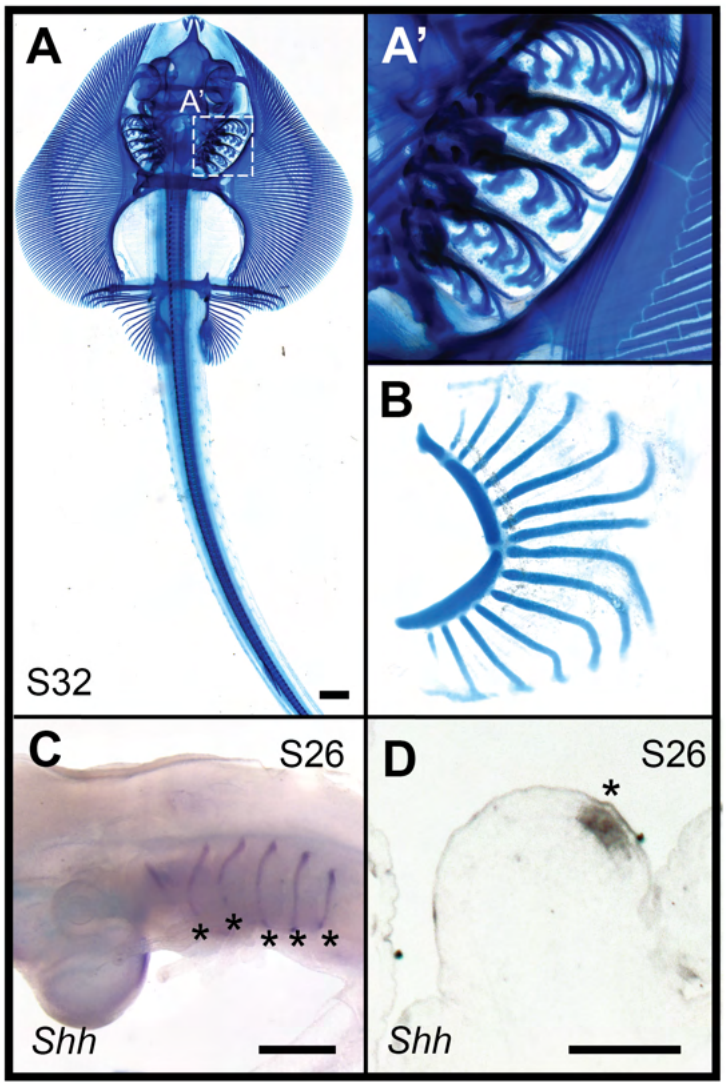

Figure 1. Overview of skate branchial ray anatomy and *Shh* expression. **(A)** Skeletal preparation of a stage (S) 32 skate embryo showing the location of the (**A**') branchial ray and gill arch cartilages *in situ*. (**B**) A dissected gill arch in frontal view shows the articulation of branchial rays with the epi- and ceratobranchial cartilages of the gill arch. **(C)** *Shh* is expressed in the gill arch epithelial ridge (GAER) of the hyoid and first four gill arches (asterisks) of skate embryos. **(D)** mRNA *in situ* hybridisation on paraffin section showing *Shh* expression within the skate GAER (asterisk). Scale bars; A:2mm, C:500µm, D:100µm.

Methods

Embryo harvesting

Skate (*L. erinacea)* embryos were obtained from the Marine Resources Center at the Marine Biological Laboratory in Woods Hole, MA, U.S.A., were reared as described in Gillis *et al.* (2012) and staged according to Ballard *et al.* (1993) and Maxwell et al. (2008). Chick (*G. gallus*) from Brown Bovan Gold hens' eggs (Henry Stewart, UK) were incubated at 38°C, and staged according to Hamburger and Hamilton (1951). Skate embryos were euthanised with an overdose of MS-222 (1g/L in seawater), and all embryos were fixed in 4% paraformaldehyde (Thermofisher) as per Gillis *et al.* (2012).

Sectioning and histochemical staining

Embryos were embedded in paraffin and sectioned at 7μm as described in O'Neill et al. (2007). Sectioned embryos were stained with Masson's Trichrome as per Witten and Hall (2003) or hematoxylin and eosin by clearing in two rinses of Histosol (National Diganostics), rehydration through serial dilutions of ethanol, staining for 15 minutes in Mayers Haematoxylin (Sigma), rinsing in running tap water for 20 minutes, rinsing briefly in 95% ethanol, and staining in 0.1% w/v Eosin Y (Sigma) in 95% ethanol for 2 minutes. Slides were then washed briefly in 95% ethanol, washed briefly with 100% ethanol, cleared with Histosol and mounted with permount (Sigma).

Lineage tracing

Labelling in both skate and chick embryos was performed *in ovo* prior to formation of the pharyngeal arches and labelled embryos were then reared until they possessed established GAER or PEM signalling centres, respectively. For skate, labelling was performed at stage (S)18, and embryos were grown to S25–29. In chick, labelling was performed at HH11, and embryos were grown to HH19–20. In both chick and skate, endodermal labelling was performed by microinjection of CellTracker™ CM-DiI (1,1'-dioctadecyl-3,3,3'3'-tetramethylindocarbocyanine perchlorate; Thermofisher), prepared as per Gillis *et al.* (2012), into the pharyngeal cavity with a pulled glass needle. In chick, ectodermal labelling was performed by application of lipid-soluble CCFSE (5-(and-6)-Carboxy-2',7'-dichlorofluorescein diacetate, succinimidyl ester; Biotium) dye to the surface ectoderm, as per Richardson *et al.* (2012) and Shone and

145 Graham (2014). Labelled embryos were embedded and sectioned as described
146 above. Sections were imaged for lineage tracing and subsequently processed for *Shh*
147 mRNA *in situ* hybridisation (ISH) for identification of the GAER/PEM.
148
149 **mRNA *in situ* hybridisation**
150 Chromogenic mRNA in situ hybridisation (ISH) was performed on paraffin sections
151 and in wholemount as described in O'Neill *et al*. (2007), with modifications according
152 to Gillis *et al.* (2012). ISH probes against skate *Shh* (GenBank EF100667) and *Fgf8*
153 (GenBank EU574737.1), and against chick *BMP7* (GenBank XM_417496.6), *SHH*
154 (GenBank NM_204821.1) and *FGF8* (GenBank NM_001012767.1) were generated
155 by *in vitro* transcription using standard methods. A plasmids for chick *BMP7* was
156 generously provided by the lab of Claudio Stern (Streit et al., 1998), and for chick *SHH*
157 and *FGF8* by the lab of Cliff Tabin (Scherz et al., 2004). Following ISH, wholemounts
158 were rinsed, post-fixed in 4% paraformaldehyde and graded into 75% glycerol for
159 imaging, while slides were rinsed in PBS, post-fixed in 4% paraformaldehyde and
160 coverslipped with DAPI-Fluoromount® G (SouthernBiotech). Third-generation mRNA
161 ISH by hybridisation chain reaction (HCR) was performed as per the Choi *et al* (2018)
162 protocol for formaldehyde fixed, paraffin-embedded sections, with modifications as per
163 Criswell and Gillis (2020). Probes, buffers, and hairpins were purchased from
164 Molecular Instruments (Los Angeles, California, USA). HCR probe set lot numners are
165 as follows: for skate *Shh* (Lot PRA753), *Ptc2* (Lot PRA754), *Fgf8* (Lot PRA755),
166 *Dusp6* (Lot PRA756), *Wnt2b* (Lot PRE300), *Wnt3* (Lot PRG814), *Wnt4* (Lot PRE301),
167 *Wnt7b* (Lot PRE302), *Wnt9b* (Lot PRE303), Notum (Lot PRG817), *Kremen1* (Lot
168 PRG816), *Axin2* (Lot PRG818), *Apcdd1* (Lot PRG815), *Col2a1* (Lot PRB574) and
169 *Sox9* (Lot PRB571); for chick *SHH* (Lot PRB282), *FGF8* (Lot PRA997), *BMP7* (Lot
170 PRb283), *WNT2B* (Lot PRG820), *WNT3* (Lot PRG823), *WNT4* (Lot PRG821), *WNT7B*
171 (Lot PRG819), *WNT9B* (Lot PRG822), *NOTUM* (Lot PRG824), *KREMEN1* (Lot
172 PRG825), *AXIN2* (Lot PRG827), *APCDD1* (Lot PRG826). All mRNA ISH experiments
173 were replicated, at minimum, in triplicate.
174
175 **Pharmacological manipulations**
176 For systemic inhibition of canonical Wnt signalling, experimental and control skate
177 embryos were reared at 15°C in petri dishes containing 50μM IWR1 (Selleck

178 chemicals) in artificial seawater or artificial seawater containing an equivalent volume
179 of vehicle (DMSO) only, respectively. IWR1 has been used previously to inhibit
180 canonical Wnt signalling in skate embryos by Nakamura et al. (2015) and in shark
181 embryos by Thiery et al. (2022). For these experiments, IWR1 was diluted to working
182 concentration from a 25mM stock solution in DMSO. Skate embryos were reared in
183 IWR1- or vehicle-containing seawater from S25 until S31/32, with drug or control
184 seawater changes every 48 hours. Once embryos reached the desired stage, they
185 were euthanised, fixed and processed for wholemount skeletal preparation according
186 to the protocol of Gillis et al. (2009a) or paraffin histology as described above.
187
188 **RNA-Seq analysis of differentially expressed genes in the GAER**
189 GAER or GAER-adjacent regions (that we termed control) of gill arch 1 were manually
190 dissected from skate embryos at S26 using tungsten needles and flash frozen in lysis
191 buffer using liquid nitrogen. In all cases, GAER and control sample pairs were
192 collected from the same arch within the same embryos, or from opposite arches within
193 the same embryo. RNA was extracted from each sample using the RNAaqueous®-
194 Micro Kit. cDNA was synthesised from extracted RNA according to the Smart-seq2
195 protocol (Picelli et al., 2014) and libraries were prepared using the Nextera XT kit
196 (Illumina). Prior to sequencing, barcoded libraries were pooled in equal proportions
197 and checked for quality, insert size and quantity using Qubit 2.0, and Agilent2100.
198 Sequencing of the 20 libraries generated was conducted by Novogene on an Illumina
199 Hi-Seq-XTen generating 150bp paired-end reads. The Cambridge Service for Data-
200 Driven Discovery (CSD3) high performance computer was used for cleaning,
201 normalisation, quality assessment, assembly, abundance quantification and
202 annotation, as per (Hirschberger et al., 2021). Raw reads were cleaned to remove
203 adapter contamination using Trim Galore v0.4.0 (parameters: --paired -q 20 –nextera),
204 for quality (Phred score 20) and minimum read length (149bp) using ea-utils tool fastq-
205 mcf (parameters: -q 20 -l 100) (Aronesty, 2011). Prior to assembly, all libraries were
206 normalised using Trinity v2.6.6 *in silico* read normalisation (Haas et al., 2013)
207 (parameters: --JM 100G --max_cov 75). Trinity v2.6.6 was used to assemble the
208 normalised reads (parameters: --seqType fq --max_memory 250G --CPU 50 --
209 min_contig_length 450) (Nishimura et al., 2017, Langmead et al., 2009, Marcais and
210 Kingsford, 2011). Basic Local Alignment Search Tool (BLAST) was used to compare
211 the assembly to the Uniprot protein database with an e-value cut-off of e-20 to search

212 for sequence similarity (Altschul et al., 1990). Transcript abundance was estimated
213 using Salmon, an alignment-free quantification method, via Trinity v2.6.6 utilities
214 (Haas et al., 2013, Patro et al., 2017). A matrix was built for each of the libraries of
215 gene-level abundance estimates (raw counts) using the Trinity
216 abundance_estimates_to_matrix.pl script. MDS principal component analysis was
217 used to check for batch effects and outliers. Individual embryo origin was a batch effect
218 and so was accordingly accounted for in the additive general linear model.
219 Differentially expressed genes between control and GAER tissue samples were
220 identified using the edgeR_3.28.0 package in R version 3.6.2 (Robinson et al., 2010)
221 using a generalised linear model likelihood ratio test (Chen, 2008) using a false
222 discovery rate of 5% and no log fold-change (LogFC) cut-off. See supplementary
223 information for assembly statistics, differential expression analysis and all R scripts
224 used. Differentially upregulated genes with a log-fold change over 2 were manually
225 screened for genes involved in known signalling pathways and transcription factors to
226 generate a list for candidate gene validation by ISH. Wnt family members were highly
227 upregulated in GAER tissue so were validated as candidate markers for the GAER
228 through third-generation ISH. Transcripts for probes in skate were based on the most
229 highly expressed isoforms.
230
231 **Imaging and figure preparation**
232 Images were taken on a Zeiss Axioscope.A1 compound microscope with a Zeiss
233 colibri 7 fluorescence LED light source using a Zeiss Axiocam 305 colour or 503 mono
234 camera and ZenPro software or a Leica M165FC stereomicroscope, a Leica DFC7000
235 T camera and LAS X software. All figures were assembled using Fiji and Adobe
236 creative cloud, with some images flipped or colours inverted for clarity and consistency
237 where needed.
238
239
240
241
242
243
244
245
246

Results

Embryonic origin and gene expression of the skate GAER

The epithelium of vertebrate pharyngeal arches derives from both ectoderm and endoderm, and the specific tissue origin of the GAER of cartilaginous fishes is not known. In the skate, *Shh* is initially expressed broadly in the anterior endodermal epithelium of each pharyngeal pouch, which subsequently gives rise to the posterior endodermal epithelium of each pharyngeal arch (Gillis and Tidswell, 2017). We speculated that the skate GAER may derive from this initially broad endodermal *Shh* expression domain, and to test this, we labelled the pharyngeal endoderm of early skate embryos by microinjection of the lipophilic dye CM-DiI (Fig.2A) into the pharyngeal cavity at stage (S)18. At this stage, the pharyngeal pouches have not yet fused with the overlying surface ectoderm, allowing for specific CM-DiI labelling of pharyngeal endodermal epithelium (Fig. 2B). Injected embryos were grown to S25–S29, by which time a GAER is established on the hyoid and gill arches and is detectable by expression of *Shh*. Of 29 embryos analysed, all retained CM-DiI label within the endodermal lining of the pharyngeal arches, and 8 showed labelling up to and including the *Shh*-expressing GAER with CM-DiI in one or more pharyngeal arches, indicating endodermal origin of these cells (Fig. 2C). Importantly, no CM-DiI labelling was ever observed in epithelial cells immediately anterior to the GAER, suggesting that this epithelium is of ectodermal origin, and that the GAER derives from endoderm at the ectoderm–endoderm interface during pharyngeal arch development.

Shh and *Fgf8* are both reported markers of the GAER (Gillis et al., 2009b), but how these expression patterns arise relative to one another through development has not been clearly shown, nor has their co-expression in the GAER been formally demonstrated. We performed chromogenic mRNA ISH on sectioned skate embryos to visualise expression of *Shh* and *Fgf8* across different stages of pharyngeal arch development. At S22 (Fig.3A,B), *Shh* is expressed in the posterior endodermal epithelium of the hyoid and gill arches (Fig.3C) consistent with previous reports (Gillis

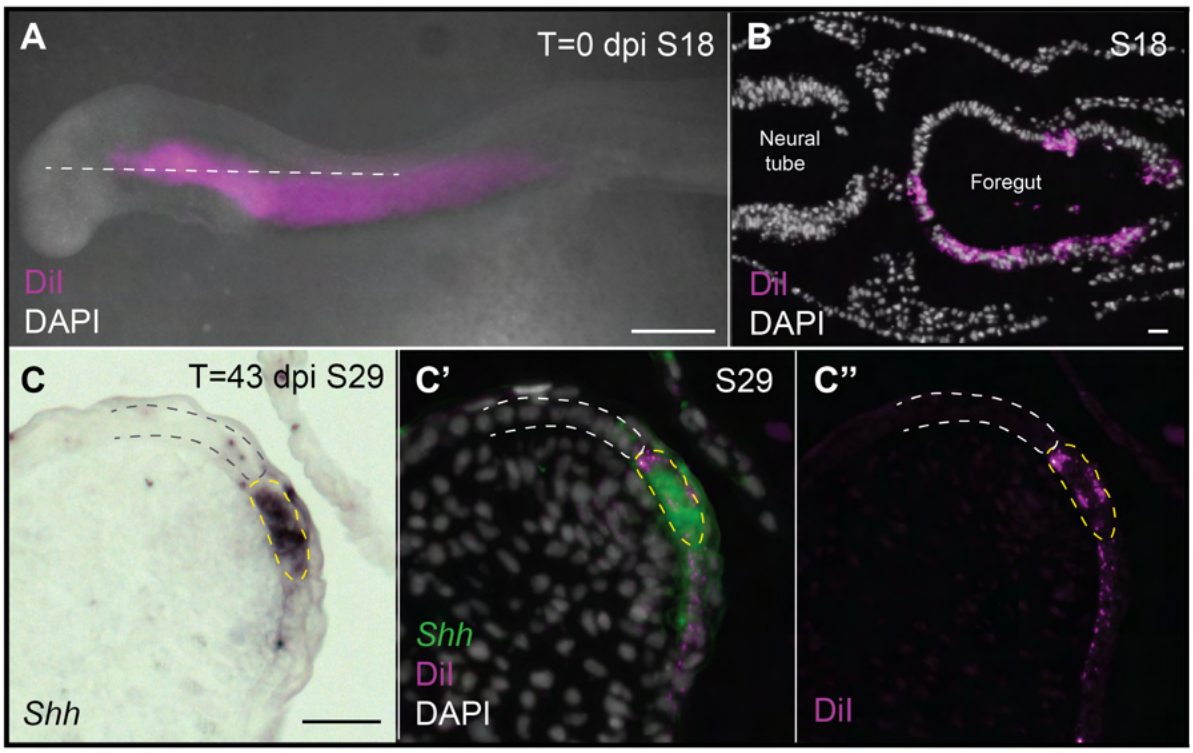

Figure 2: Endodermal origin of the skate GAER. (**A**) Microinjection of CM-DiI into the pharyngeal cavity of skate embryos at S18 results in (**B**) specific labelling of the pharyngeal endoderm. (**C**) *Shh* is a marker of the GAER (dashed yellow line) in CM-DiI-labelled embryos, and (**C', C''**) Co-localisation of CM-DiI and *Shh* expression indicates that the cells of the GAER are of endodermal origin. Dashed white outline demarcates GAER-adjacent (and presumed ectodermal) epithelium that is never labelled with CM-DiI. (**C**), (**C'**), and (**C''**) are the same section, imaged sequentially for *Shh* expression and CM-DiI retention. A–P: Anterior–posterior axis, dpi: days post injection. Scale bars; A: 500μm, B–C: 20μm.

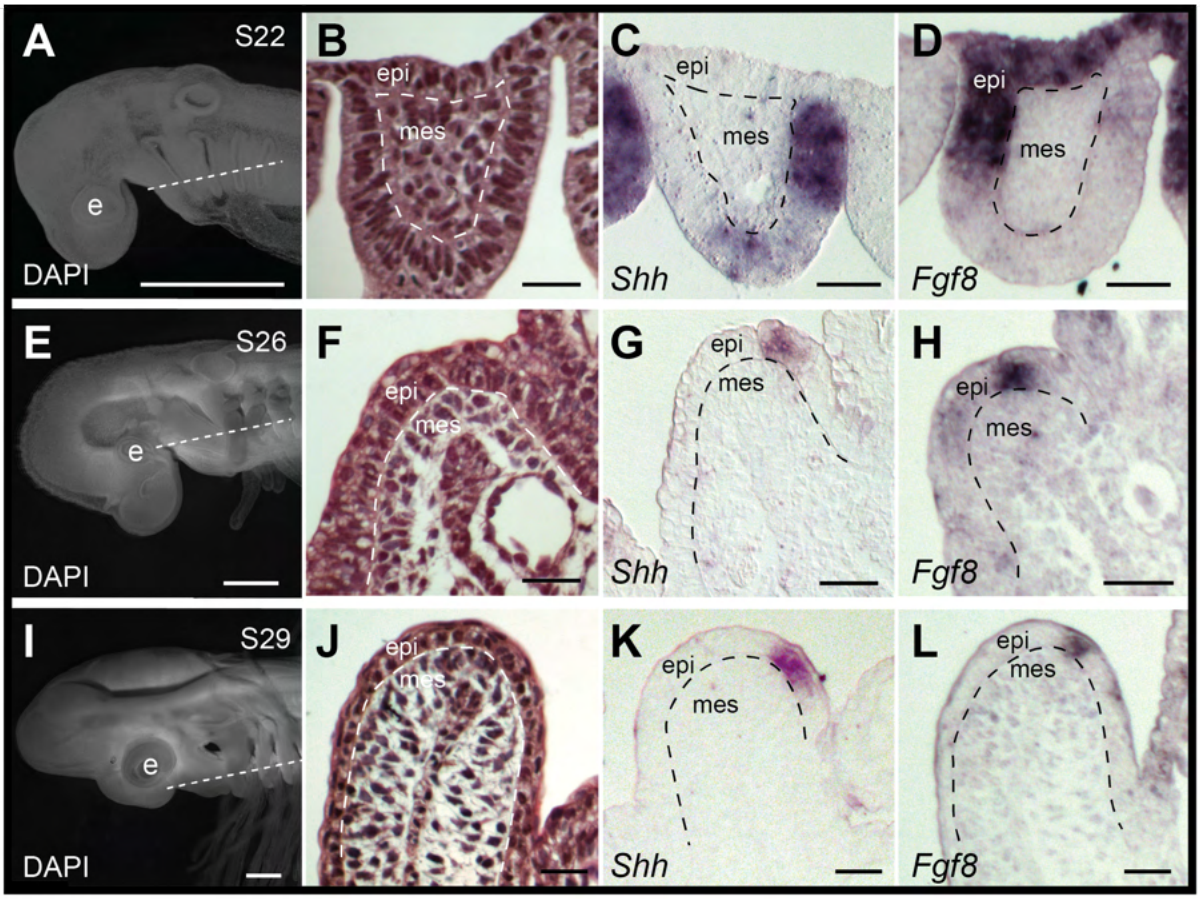

Figure 3: Expression of *Shh* and *Fgf8* in developing skate pharyngeal arches. (**A**) At S22, (**B**) the pharyngeal arches are delineated by endodermal pouches that are contacting or fusing with overlying surface ectoderm. At this stage, (**C**) *Shh* is expressed in the posterior endodermal epithelium of the developing hyoid and gill arches, while (**D**) *Fgf8* is expressed in the anterior endodermal and lateral ectodermal epithelium of each arch. (**E**) By S26, (**F**) the hyoid and gill arches are expanding laterally, and (**G**) *Shh* and (**H**) *Fgf8* are both expressed in a ridge of epithelial cells along the leading edge of the expanding arches. (**I-L**) These gene expression features persist until S29. E: eye, Epi: epithelial, Mes: mesenchymal, S: stage. Scale bars; A,E,I: 1mm, all others: 40 μm.

313 and Hall, 2016, Gillis and Tidswell, 2017) whereas *Fgf8* is expressed in the anterior
314 endoderm and lateral ectoderm of these arches (and also weakly in the distal arch
315 endodermal epithelium, partially overlapping with *Shh*) (Fig. 3D). By S26 (Fig.3E,F),
316 *Shh* (Fig.3G) and *Fgf8* (Fig.3H) transcripts both resolve to a thin ridge of epithelial
317 cells (the putative GAER) along the leading edge of the expanding hyoid and gill
318 arches, and these expression patterns persist until S29 (Fig.3I–L). Using multiplexed
319 ISH by HCR at S26, we found that *Shh* and *Fgf8* are precisely co-expressed in the
320 GAER of the expanding hyoid and gill arches (Fig.4A–A''). To determine which tissues
321 are transducing signals from the GAER, we performed ISH by HCR for *Ptc2* and
322 *Dusp6* – transcriptional readouts of Shh and MAP kinase-mediated FGF signalling,
323 respectively (Pearse et al., 2001, Kawakami et al., 2003). Consistent with previous
324 reports (Gillis and Hall, 2016), we observed *Ptc2* expression predominantly within the
325 posterior arch environment, including within the GAER and adjacent epithelia as well
326 as within posterior-distal arch mesenchyme and core mesoderm (Fig.4B–B''). In
327 contrast, *Dusp6* is expressed more specifically within the GAER and broadly
328 throughout underlying distal arch mesenchyme (Fig.4C–C''). Altogether, these
329 findings demonstrate that the GAER is a signalling centre of endodermal origin, and a
330 source of both Shh and Fgf8 signals, with the former transduced preferentially within
331 in the posterior arch environment, and the latter more broadly throughout distal arch
332 mesenchyme.
333
334 **Conservation of embryonic origin and gene expression in a chick pharyngeal**
335 **arch signalling centre**
336 In amniotes, the 2nd (hyoid) pharyngeal arch undergoes a prolonged phase of lateral
337 expansion, with this arch eventually fusing with the posterior ectoderm to close the
338 neck. Chick embryos possess a ridge of *SHH*-expressing epithelial cells along the
339 leading edge of the expanding hyoid arch, and this ridge has been termed the posterior
340 ectodermal margin (PEM) (Wall and Hogan, 1995). The PEM is reminiscent of the
341 GAER of cartilaginous fishes, and to test whether these structures share common
342 tissue origins and gene expression features, we conducted a parallel set of lineage
343 tracing and gene expression analyses of the PEM in chick embryos. To test the germ
344 layer origin of the PEM, we first traced the fate of the pharyngeal ectoderm by *in ovo*
345 topical application of the lipid-soluble dye CCFSE (Richardson et al., 2012,

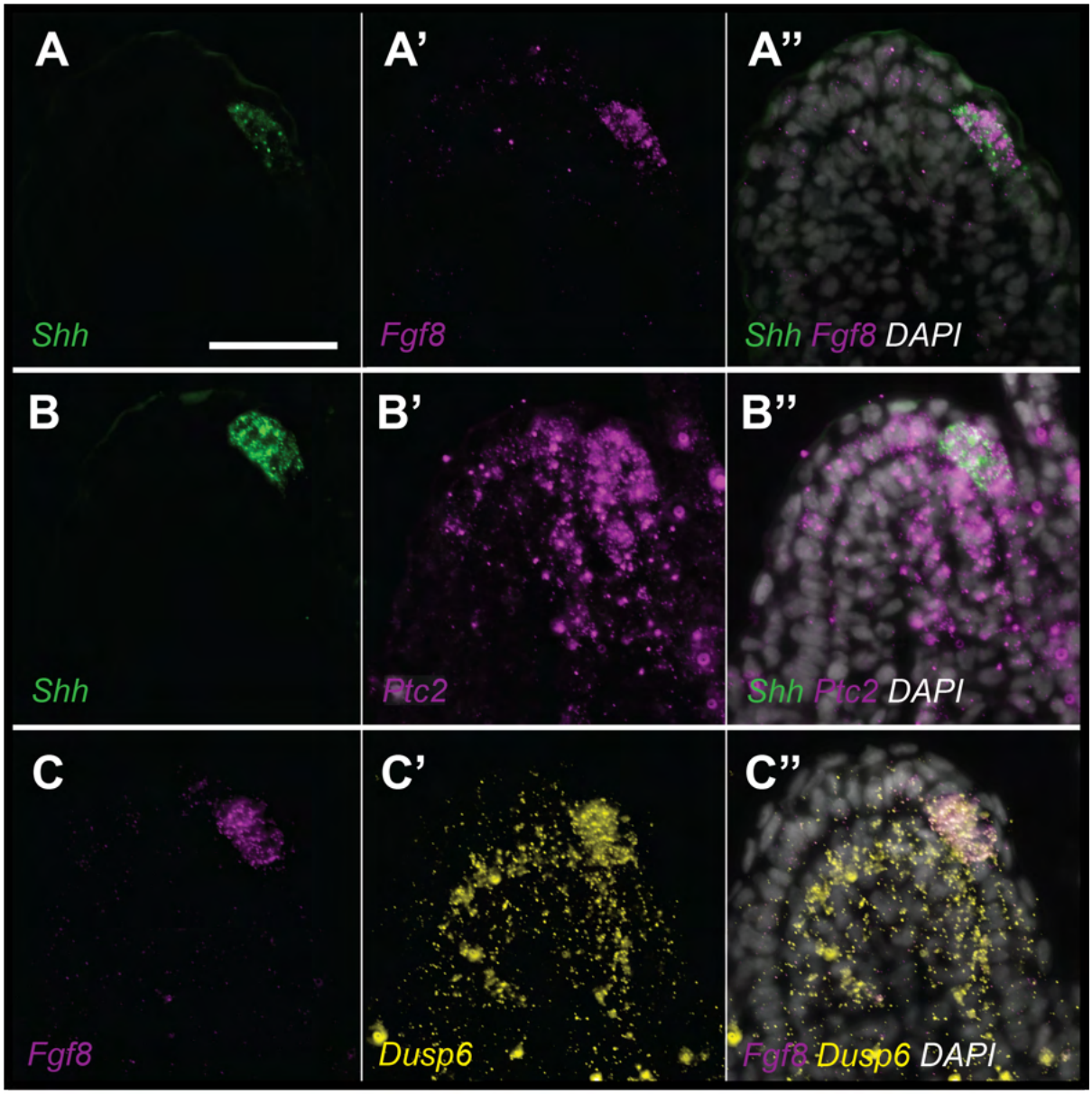

Figure 4: Expression of *Shh* and *Fgf8* signalling components in skate gill arches. ISH by HCR shows co-expression of (**A**) *Shh* and *Fgf8* in the skate GAER at S26**.** (**B**) *Ptc2* serves as a transcriptional readout of Shh signal transduction, and is expressed in the posterior arch environment, including in the GAER and adjacent epithelia, and in posterior–distal mesenchyme and core mesoderm. (**C**) *Dusp6* expression indicates MAP kinase-mediated Fgf signal transduction within the GAER and broadly throughout distal arch mesenchyme. Scale bar: 50μm.

358 Shone and Graham, 2014). Of 29 embryos labelled at HH11, all showed some
359 labelling of the ectoderm-derived lining of the pharyngeal arches by HH19, with 9
360 embryos showing strong labelling of the ectoderm-derived epithelium of the hyoid arch
361 up to, but excluding, the *SHH*-expressing cells of the PEM (Fig. 2 Supplement 1A–C).
362 We next traced the fate of pharyngeal endoderm by microinjection of CM-DiI into the
363 pharyngeal cavity. Of 37 embryos labelled at HH11, all retained some CM-DiI labelling
364 within the endoderm-derived epithelium of the pharyngeal arches, with 9 embryos
365 showing CM-DiI labelling of the endodermal lining of the hyoid arch up to and including
366 the *SHH*-expressing PEM (Fig. 2 Supplement 1D–E). These findings point to an
367 endodermal origin of the PEM, with this signalling centre forming at the endoderm-
368 ectoderm boundary of the hyoid arch epithelium. *SHH, FGF8* and *BMP7* are all
369 reported markers of the PEM in chick (Wall and Hogan, 1995), and we confirmed that
370 while *SHH* and *BMP7* are initially expressed broadly in the pharyngeal endoderm and
371 *FGF8* in the pharyngeal ectoderm and endoderm of the hyoid arch (Fig. 3 Supplement
372 1A–J), expression of all three genes subsequently resolves to a discrete epithelial
373 domain along the leading edge of the expanding arch (Fig. 3 Supplement 1K–T).
374 Finally, we found using ISH by HCR that *SHH, FGF8* and *BMP7* are co-expressed
375 within cells of the PEM (Fig. 3 Supplement 1U). These findings demonstrate that the
376 skate GAER and chick PEM share embryonic tissue origins and expression patterns
377 of signalling molecules through development and are therefore homologous and an
378 ancestral feature of the pharyngeal arche(s) of jawed vertebrates.
379

380 ***Wnt* gene expression in the skate GAER and GAER-adjacent ectoderm**

381 In an attempt to discover additional gene expression features of the GAER, we
382 conducted a transcriptomic and differential gene expression analysis between the
383 GAER and non-GAER regions of the first gill arch of skate embryos. Briefly, we
384 manually dissected the posterior–distal GAER region and non-GAER (control) region
385 from the first gill arch of S26 skate embryos (n=5) (Fig.5), and we performed RNA
386 extraction, library preparation, and RNAseq analysis on these samples. Following *de*
387 *novo* transcriptome assembly, we compared gene expression levels between GAER
388 and control tissue and using a false discovery rate of 5% and no log fold-change
389 (LogFC) cut-off we generated a list of 401 genes that were upregulated in the GAER.
390 We sorted this list for genes encoding signalling pathway components and

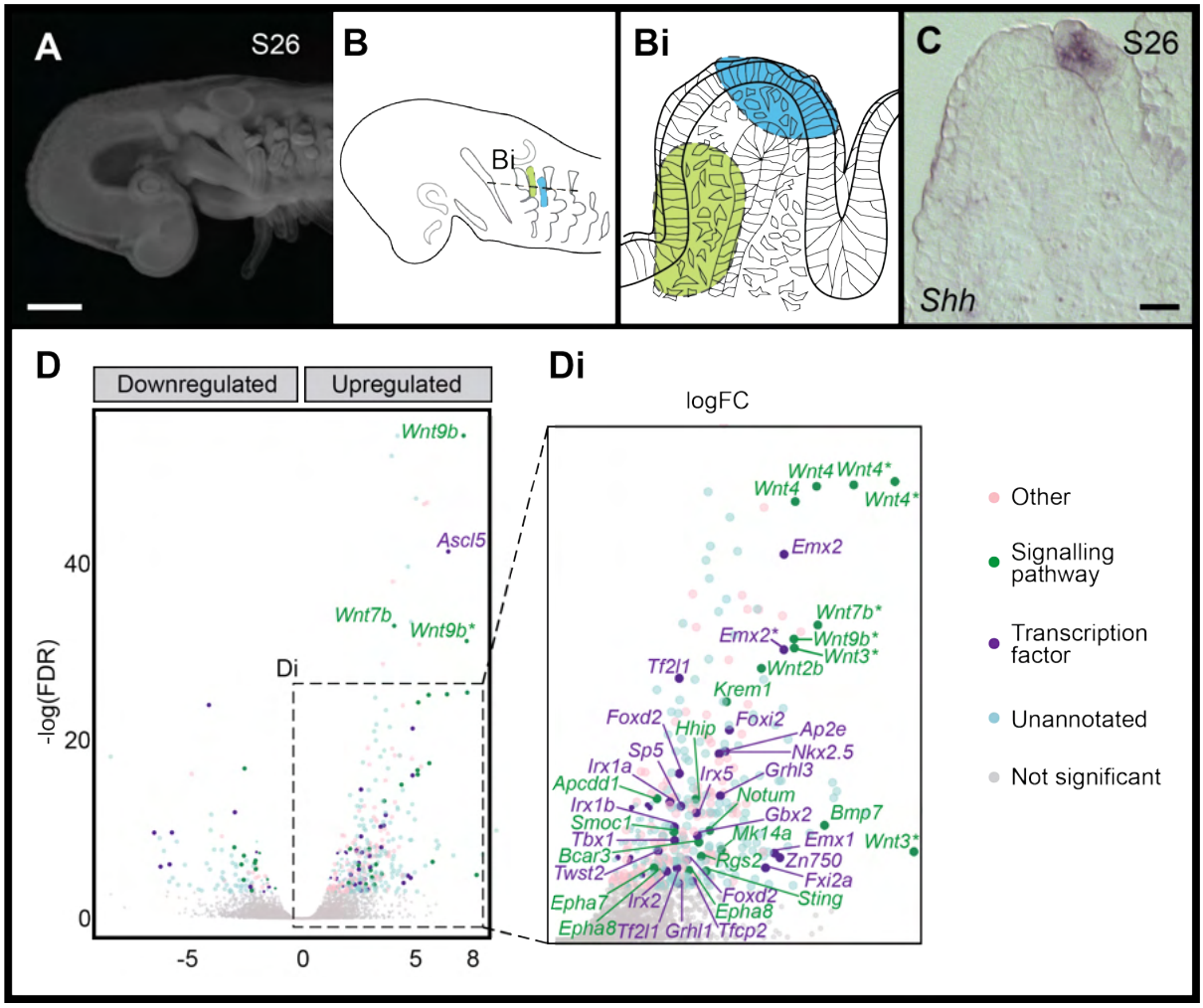

Figure 5: RNA-seq and differential gene expression analysis of GAER and non-GAER gill arch tissues in S26 skate embryos. (**A**) DAPI stained skate embryo at S26 and (**B**) schematic of dissection from gill arch 1 of (**Bi**) non-GAER (control) tissue region (green) and posterior–distal GAER tissue region (blue), as guided by (**C**) *Shh* expression. (**D, D^{i}**) Volcano plot illustrating differential gene expression between GAER and non-GAER tissues. Genes with >2 logFC and <0.05 false discovery rate (FDR) are highlighted and assigned functional category using colour coding as per key. Genes with >2 logFC are shown in larger point size. Signalling molecules and transcription factors with >2 logFC and <0.05 FDR are labelled (* denotes manual annotation of sequence). Differential expression was determined using edgeR with a general linear model and likelihood ratio test, corrected for multiple testing using the Benjamin-Hochberg method to control the FDR. Scale bars; A:1mm C: 50μm.

406 transcription factors with a log-fold change >2 (Fig.5E) and found several components
407 of the Wnt signalling pathway among genes upregulated in GAER tissue. These
408 included genes encoding the Wnt ligands Wnt2b, Wnt3, Wnt4, Wnt7b and Wnt9, the
409 transmembrane Wnt inhibitors Kremen1 (Mao et al., 2002) and Adenomatosis
410 Polyposis Coli Down-regulated 1 (APCDD1) (Shimomura et al., 2010), and the
411 secreted Wnt antagonist Notum (Zhang et al., 2015). We chose to further investigate
412 potential involvement of the Wnt pathway in GAER signalling by spatially validating
413 the expression of these genes, using the most highly expressed isoforms for HCR
414 probe set design.
415
416 To characterise expression of genes encoding Wnt ligands relative to *Shh* expression
417 in the GAER, we used multiplexed ISH by HCR to visualise transcript localisation in
418 sections of S26 skate gill arches. We found that while *Wnt7b* was co-expressed
419 with *Shh* in the cells of the GAER (Fig. 6A, A'), *Wnt2b*, *Wnt3*, *Wnt4* and *Wnt9b* were
420 all expressed predominantly in the ectoderm immediately adjacent to the GAER (Fig.
421 6B–E). We next examined the expression of the Wnt signalling downstream target
422 genes and found that *Apcdd1* was expressed in the GAER and anterior–distal
423 mesenchyme (Fig. 6F), *Notum* in the anterior–distal mesenchyme (Fig. 6G)
424 and *Kremen1* in the anterior (GAER-adjacent) ectoderm (Fig. 6H). Finally, broad
425 transcription of *Axin2* throughout distal gill arch tissues (Fig. 6I) indicates that Wnt
426 signalling within this territory is occurring through the canonical/β-catenin pathway
427 (Lustig et al., 2002). While these findings do not allow us to attribute expression of
428 specific readouts to signalling by particular Wnt ligands, our spatial expression data
429 nevertheless indicate that some Wnt signals emanating from the GAER or GAER-
430 adjacent ectoderm are transduced preferentially within the anterior arch environment,
431 in a pattern complimentary to the posterior epithelial and mesenchymal transduction
432 of Shh signals from the GAER.
433
434 **Conservation of *WNT* gene expression in PEM-adjacent ectoderm in chick**
435 To test whether the Wnt gene expression patterns described above for skate are a
436 unique feature of cartilaginous fishes or a general feature of jawed vertebrates, we
437 again used ISH by HCR to visualise expression in or around the hyoid arch PEM in

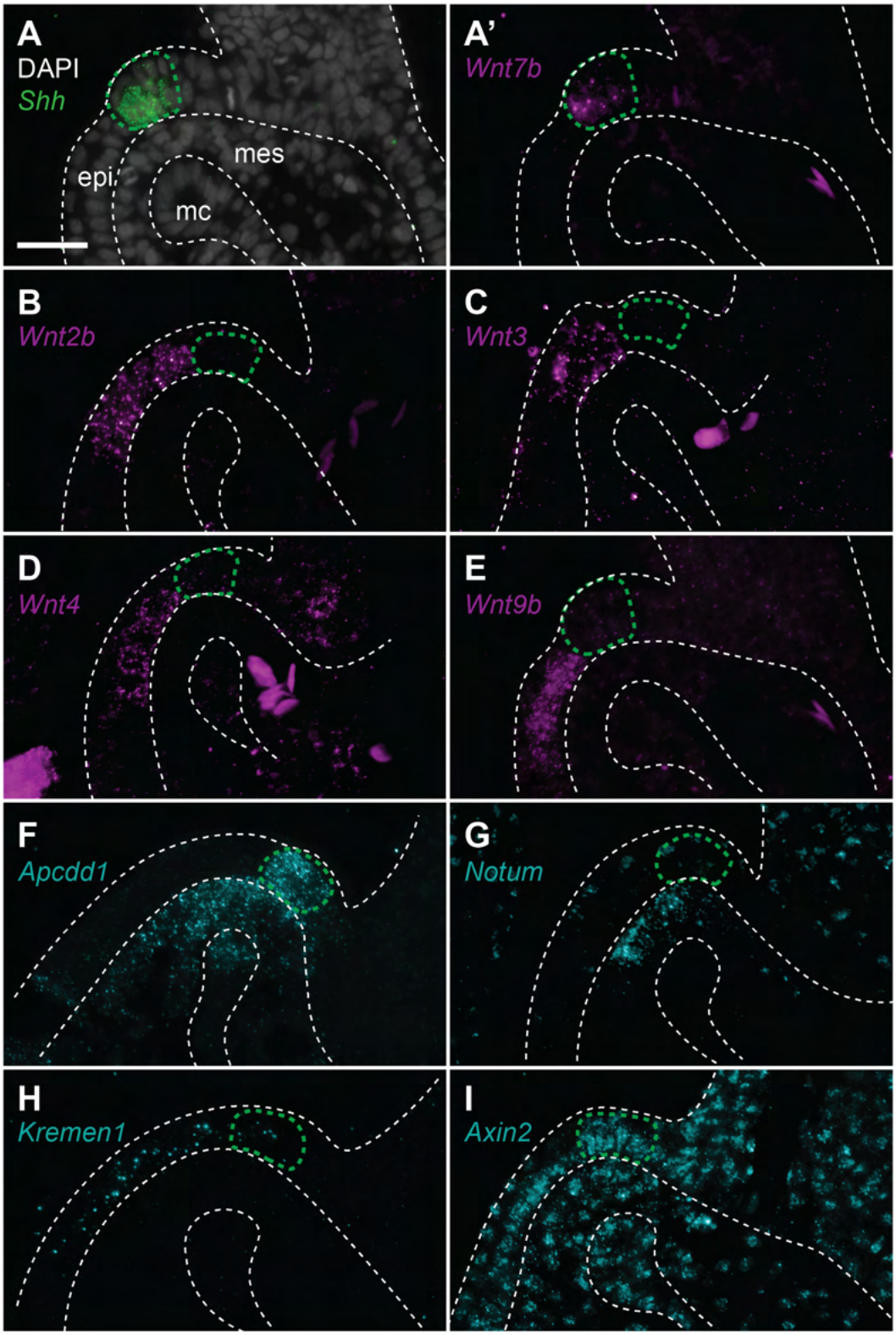

Figure 6: *Wnt* pathway genes are expressed in and around the GAER in skate. In S26 skates, (**A**) ISH by HCR for *Shh* and DAPI staining was performed alongside each gene of interest as a marker of the GAER and for general tissue overview, respectively. For ease of visualisation in **A'–I**, *Shh* expression is not shown but GAER

443 cells are outlined green, and arch tissues are outlined in white. (**A'**) *Wnt7b* is co-
444 expressed with *Shh* in the GAER. (**B)** *Wnt2b,* **(C)** *Wnt3*, **(D)** *Wnt4* and **(E)** *Wnt9b* are
445 predominantly expressed in the ectodermal epithelium immediately adjacent the
446 GAER. (**F**) *Apcdd1* is expressed in the GAER, and also in the anterior–distal
447 mesenchyme underlying the GAER. (**G**) *Notum* is expressed in the anterior–distal arch
448 mesenchyme. (**H**) *Kremen1* is expressed in the GAER and in GAER-adjacent
449 ectodermal epithelium. (**I**) Broad *Axin2* expression in the vicinity of *Wnt*-expressing
450 epithelium indicates signalling through the canonical Wnt signalling pathway. Epi:
451 epithelial, mes: mesenchymal, mc: mesodermal core. Scale bar: 50μm.

452
453
454
455
456
457
458
459
460
461
462
463
464
465
466
467
468
469
470
471
472
473
474
475

476 chick embryos (Fig. 6 Supplement 1A). At HH20, we found that *WNT2B, WNT3, WNT4*
477 and *WNT9B* are all predominantly expressed in the ectodermal epithelium directly
478 adjacent to the PEM (Fig. 6 Supplement 1B–E). Unlike in skate, *WNT2B* expression
479 in chick extends into the PEM, and we were unable to detect expression of *WNT7B* in
480 the PEM. We also found that *APCDD1* is expressed in the distal arch mesenchyme
481 (Fig. 6 Supplement 1F), *NOTUM* in the anterior–distal mesenchyme and the PEM (Fig.
482 6 Supplement 1G), and *KREMEN1* predominantly in the ectodermal (PEM-adjacent)
483 epithelium (Fig. 6 Supplement 1H). Broad transcription of *AXIN2* was also seen in the
484 distal arch tissues, indicating active canonical/β-catenin pathway Wnt signalling (Fig.
485 6 Supplement 1I). These findings demonstrate that Wnt signalling emanating
486 predominantly from PEM- or GAER-adjacent ectoderm is conserved in chick and
487 skate, respectively, and is therefore likely an ancestral feature of the developing
488 pharyngeal arches of jawed vertebrates.
489
490 **Wnt suppresses GAER Shh signal transduction and inhibits cartilage**
491 **formation in the anterior gill arch in skate**
492 To explore the function of Wnt signalling during skate pharyngeal arch development,
493 we inhibited canonical Wnt signalling in skate embryos using IWR1, a small molecule
494 tankyrase inhibitor that antagonises Wnt signalling by stabilising the Axin/β-catenin
495 destruction complex (Lu et al., 2009, Kulak et al., 2015). Briefly, skate embryos were
496 maintained in a bath of 50μM IWR1 or vehicle-only control (DMSO) in seawater from
497 S25 for 72h to assess gene expression changes in response to drug treatment, or for
498 6–8 weeks (until S31/32) to assess effects of Wnt signalling inhibition on gill arch
499 skeletal patterning, with replacement of drug- or control-seawater every 48h. IWR1-
500 treated embryos showed a marked reduction in the expression of *Axin2* throughout
501 their gill arches (Fig. 6 Supplement 2A–B), as well as a reduction in the expression of
502 *Apcdd1* in the GAER and anterior–distal gill arch mesenchyme (Fig. 6 Supplement
503 2C–D) and a complete loss of *Notum* expression in anterior–distal gill arch
504 mesenchyme (Fig. 6 Supplement 2E–F). These findings indicate that our drug
505 treatment effectively supressed canonical Wnt signalling from the GAER and GAER-
506 adjacent epithelium, including those signals transduced asymmetrically in the anterior
507 gill arch environment.
508

509 Shh is a pro-chondrogenic signal from the GAER in skate gill arches (Gillis et al.,
510 2009b), and this signal is transduced asymmetrically with the posterior gill arch
511 environment (Gillis and Hall, 2016, and see above). To test whether anteriorly-
512 transduced Wnt signalling may act to restrict Shh signal transduction to the posterior
513 gill arch, we examined expression of *Shh* and *Ptc2* in skate embryos 72h after the
514 onset of IWR1 treatment. While we observed no noticeable change in the expression
515 of *Shh* or in the spatial distribution of *Ptc2* transcripts in gill arch mesenchyme with
516 IWR1 treatment, we did note a qualitative increase in *Ptc2* expression within the
517 normal mesenchymal domain, and a striking anterior expansion of *Ptc2* expression
518 within the epithelium adjacent to the GAER (Fig.7A–D). To quantify this epithelial
519 expansion, we compared the mean number of *Ptc2*+ cells anterior to the *Shh*-
520 expressing GAER across two or three sections at equivalent positions in DMSO
521 control (n=3) or IWR1 (n=4) treated embryos and found a significant anterior
522 expansion of *Ptc2* expression within the epithelium adjacent to the GAER in IWR1
523 treated embryos (Fig.7E–G; P= 0.036). This points to a role for GAER-adjacent Wnt
524 signalling in restricting the transduction of pro-chondrogenic Shh signalling in the
525 anterior gill arch territory in skate.
526
527 Finally, to test for an effect of Wnt inhibition on the gill arch skeleton, we examined
528 skeletal morphology in skate embryos reared in DMSO control seawater or IWR1 from
529 S25–S31/32. The skate hyoid and gill arch skeleton include branchial rays that
530 articulate exclusively with the posterior margin of the gill arch cartilages, and that
531 invariably develop on the posterior side of the mesodermally-derived interbranchial
532 muscle plate that extends down the middle of the arch (Daniel, 1934, Gillis et al.,
533 2009a). Skate embryos reared in DMSO control seawater showed no gill arch skeletal
534 defects (n=4 embryos; Fig. 8A–Ai), while embryos reared in IWR1 seawater
535 possessed conspicuous ectopic branchial rays in the anterior gill arch territory (n= 7/8
536 embryos; Fig. 8B–Bi). These ectopic branchial rays occurred along the entire
537 dorsoventral axis of the arch and ranged from short cartilage rods located in the
538 anterior–distal gill arch to nearly full-length branchial rays that extended much of the
539 way toward the gill arch cartilages. In section, normal branchial rays of skate embryos
540 reared in DMSO control seawater always developed on the posterior side of the
541 mesodermally-derived interbranchial muscle plate of each gill arch: this was evident

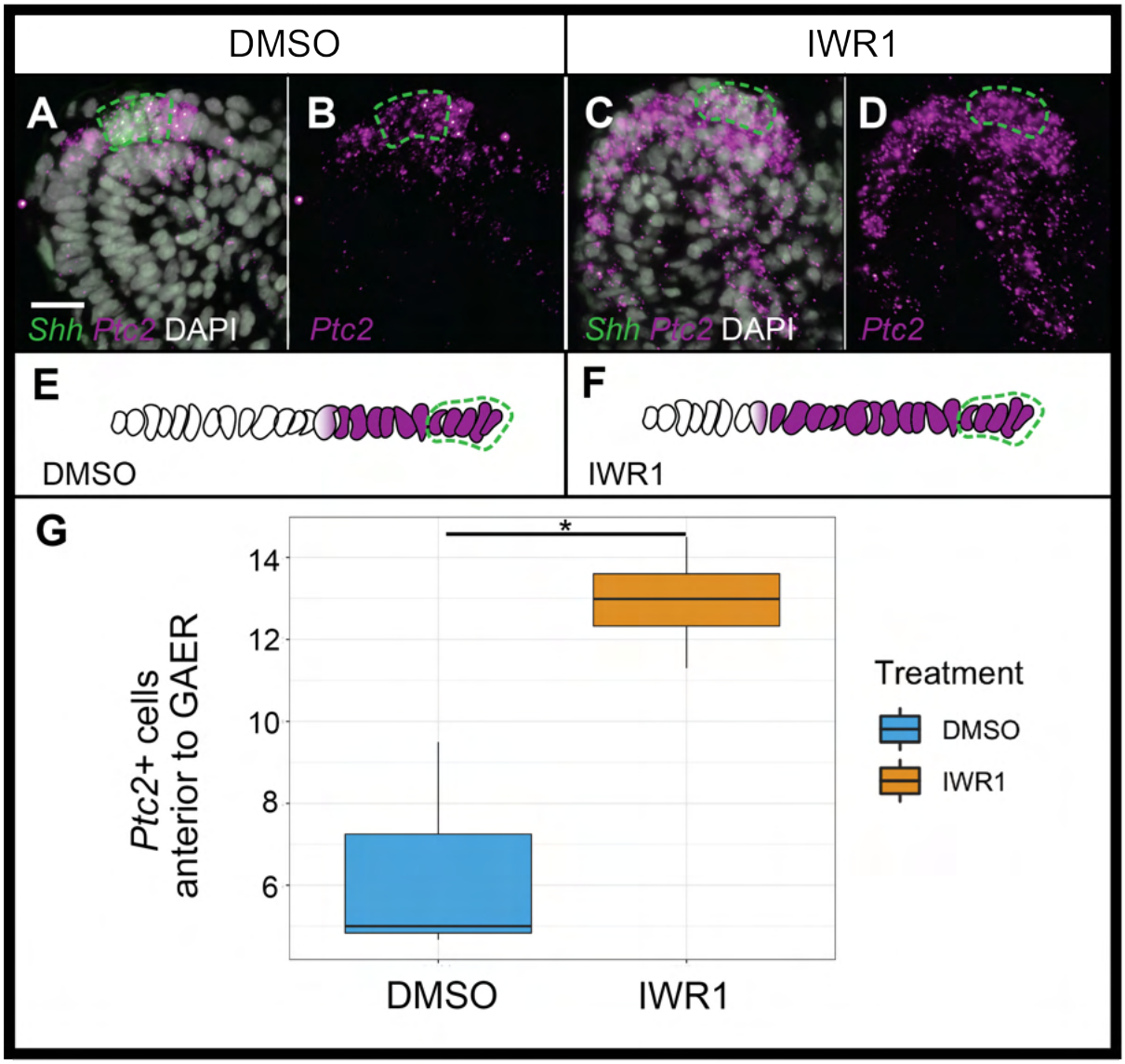

Figure 7: Wnt signalling restricts transduction of GAER Shh signalling to the posterior gill arch environment. ISH by HCR on sections of skate embryos treated for 72 hours with (**A,B**) DMSO or (**C,D**) IWR1 shows no difference in *Shh* expression but an expansion of *Ptc2* expression within the epithelium anterior to the *Shh*-expressing GAER. **(E)** Schematic illustration of the mean number of cells containing *Ptc2* transcripts anterior to the GAER in DMSO control (n=3; 6.3 cells) or (**F**) IWR1 treated (n=4; 12.94 cells) embryos, using the mean cell count of two or three sections at equivalent positions in the gill arch from each embryo. (**G**) A significant increase in *Ptc2*+ cells in the epithelium anterior to the GAER in IWR1 treated embryos compared to control (P= 0.036; t test). In **A–F**, *Shh* expression is indicated by green dashed line. Images in **A–D** taken using identical exposure settings. Scale bar: 20 μm.

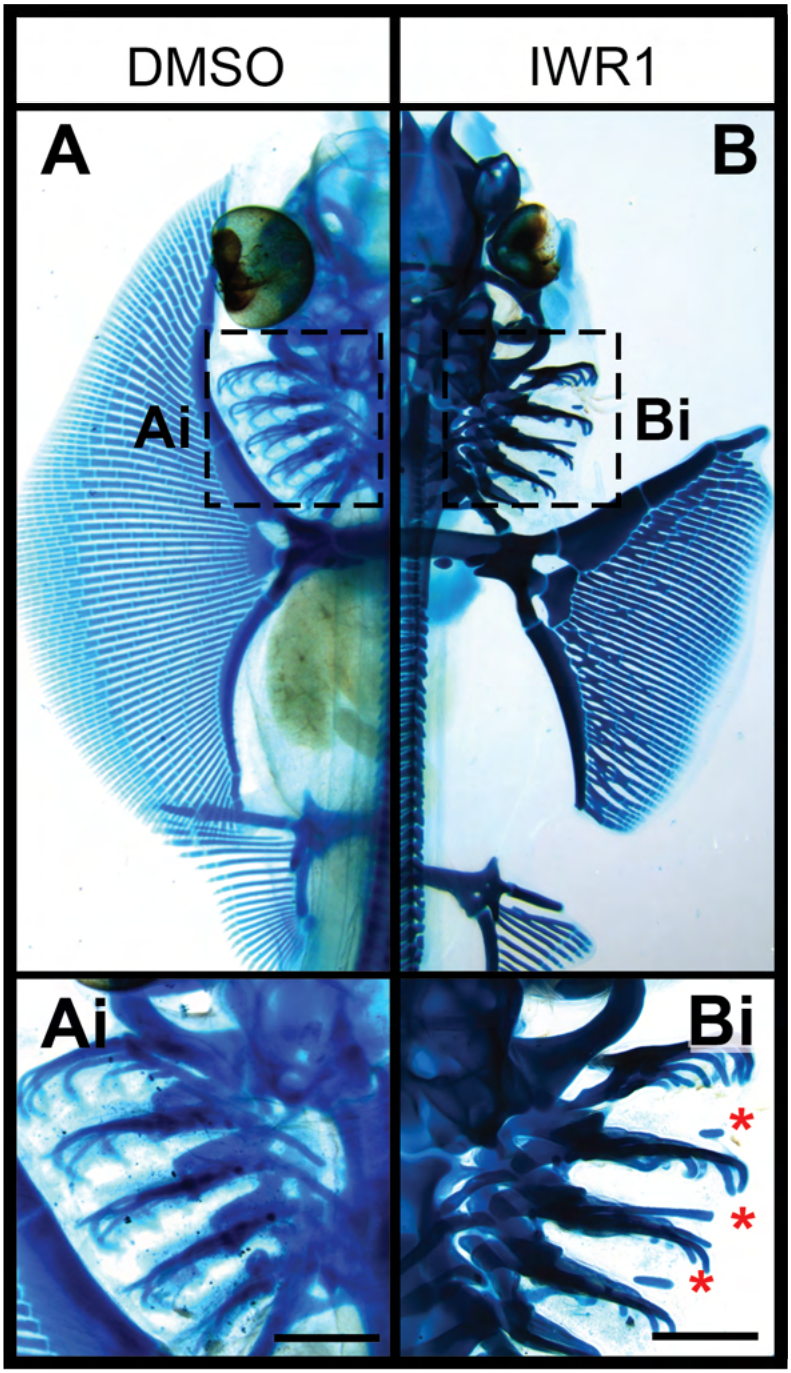

Figure 8: Ectopic branchial ray formation upon inhibition of Wnt signalling. (A) In control (DMSO) skate embryos, branchial rays (magnified in **Ai**) articulate exclusively with the posterior margin of the gill arches. **(B)** Embryos reared in the Wnt inhibitor IWR1 possessed ectopic branchial rays (magnified in **Bi**) that were embedded within connective tissue of the anterior gill arch (ectopic rays present in n=7/8 embryos examined; indicated by red asterisk). Scale bars: 500 μm.

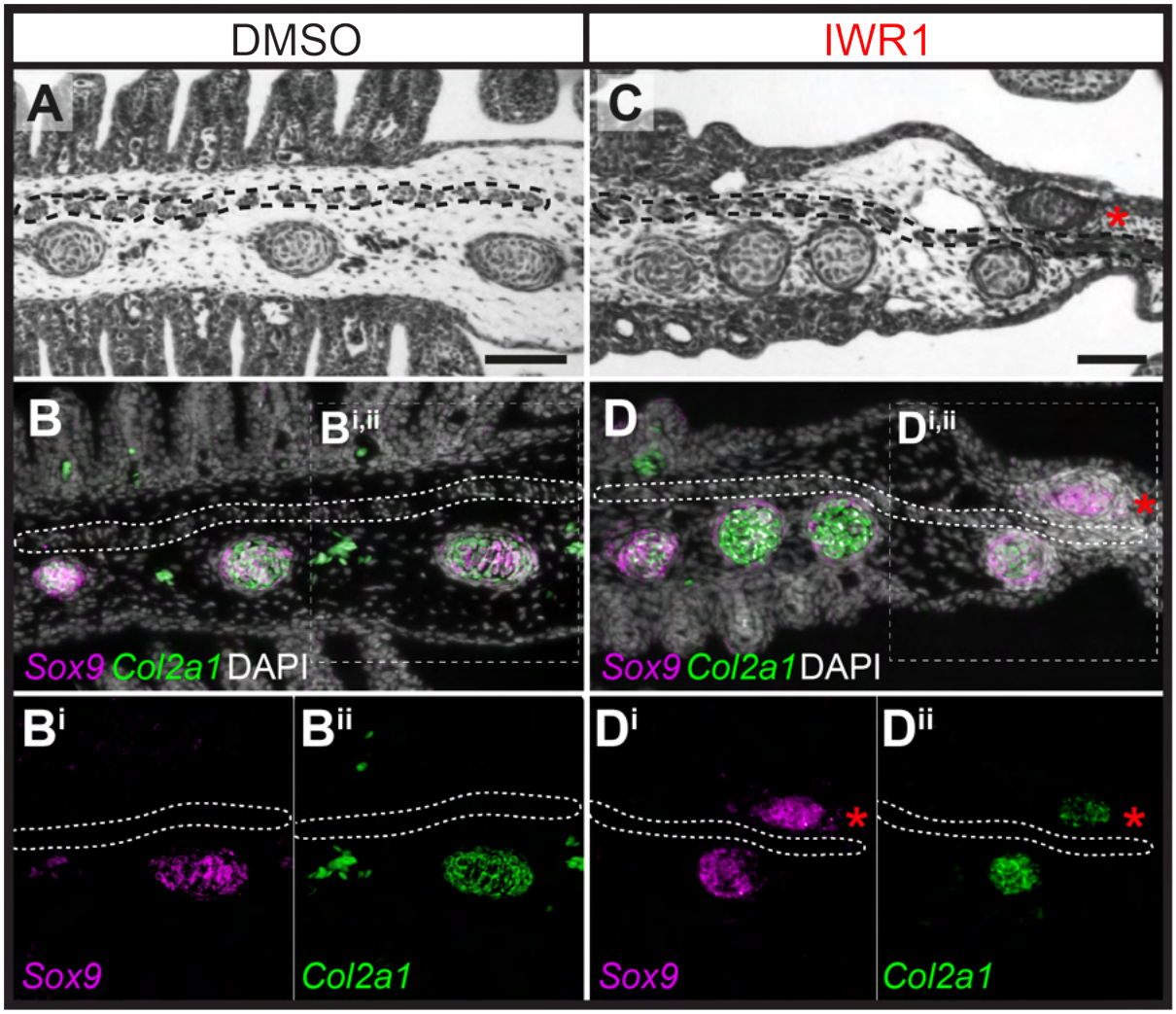

Figure 9: Repression of cartilage development in the anterior gill arch by Wnt signalling. (A) Section of the branchial rays of control (DMSO) skate embryos, showing they develop exclusively on the posterior side of the interbranchial muscle plate, as is evident from histochemical staining and **(B–ii)** ISH by HCR for the chondrocyte markers *Sox9* and *Cola2a1*. **(C)** Section of the branchial rays of embryos reared in the Wnt inhibitor IWR1 show ectopic branchial rays form anterior to the interbranchial muscle plate, as evident from histological analysis and **(D–Dii)** ISH by HCR for *Sox9* and *Col2a1*. Red asterisks indicate ectopic branchial rays, and interbranchial muscle plate is outlined with a dashed line. Scale bars: 50 μm.

582 from histochemical staining (Fig. 9A) and from HCR for the chondrocyte markers *Sox9*
583 and *Col2a1* (Fig. 9B). Conversely, in skate embryos reared in IWR1 seawater, ectopic
584 branchial rays were consistently located anterior to the interbranchial muscle plate
585 (Fig. 9C–D). The induction of ectopic branchial rays with IWR1 treatment suggests
586 that Wnt signalling contributes to the maintenance of anteroposterior polarity of the
587 skate gill arch skeleton by repressing chondrogenesis in the anterior gill arch and may
588 do so by restricting transduction of GAER Shh signalling to the posterior gill arch
589 territory.
590

591 # Discussion

592

593 The molecular mechanisms governing spatial regulation of cell fate decisions are
594 crucial to the establishment and maintenance of anatomical polarity within
595 developing tissues and organs. Here, we show that the GAER signalling centre that
596 forms on the hyoid and gill arches of cartilaginous fishes is of endodermal origin,
597 arising precisely at the boundary of surface ectoderm and pharyngeal endoderm,
598 and that pro-chondrogenic Shh signals from the GAER are transduced preferentially
599 within the posterior gill arch environment. We further show that the ectoderm
600 immediately anterior and adjacent to the GAER is a signalling centre that expresses
601 several Wnt family genes, and that Wnt signals from this centre are transduced
602 preferentially in the anterior arch environment. Pharmacological inhibition of
603 canonical Wnt signalling in skate embryos leads to an expansion of Shh signal
604 transduction within the anterior territory of the gill arch, and to the formation of
605 ectopic anterior branchial ray cartilage, highlighting Wnt–Shh signalling antagonism
606 across an ectodermal–endodermal tissue boundary as a key molecular regulator of
607 cell fate determination and anatomical polarity with the developing gill arch skeleton
608 (Fig. 10).
609

610 Previous analyses have reported the expression of several Wnt genes in developing
611 craniofacial tissues of bony vertebrates (Summerhurst et al., 2008), including
612 expression of *WNT2B* and *WNT9B* in the pharyngeal arch ectoderm of the chick
613 (Geetha-Loganathan et al., 2009), *Wnt9b* in the first and second pharyngeal arches in
614 zebrafish (Jezewski et al., 2008), and *Wnt4a* in zebrafish pharyngeal ectoderm (Choe

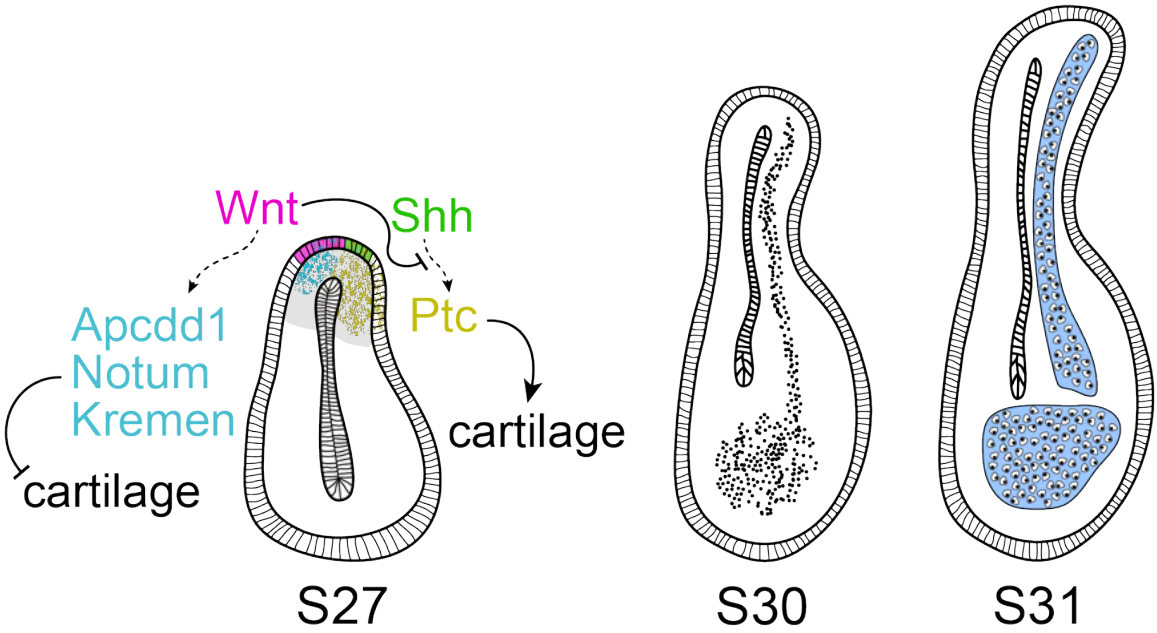

Figure 10: Wnt and Shh signalling and cell fate determination in skate gill arches. Shh signalling from the endodermally-derived GAER is transduced within the posterior-distal gill arch environment, where it promotes the differentiation of cartilaginous branchial rays. Wnt signals from ectoderm adjacent to the GAER are transduced within the anterior–distal gill arch environment, where they repress Shh signal transduction and inhibit cartilage formation in the anterior gill arch.

635 et al., 2013). While β-catenin-independent (i.e. non-canonical) Wnt signalling plays a
636 crucial role in epithelial remodelling during the early formation of pharyngeal
637 endodermal pouches in zebrafish (Choe et al., 2013), canonical Wnt signalling has
638 been implicated in patterning of the pharyngeal arch-derived skeleton in multiple taxa.
639 Blocking canonical Wnt signalling causes disrupted facial cartilage formation,
640 including reductions of Meckel's and ceratohyal cartilages in zebrafish (Alexander et
641 al., 2014) and loss of ectodermal canonical Wnt signalling in mice causes loss of facial
642 bones with hypoplasia of all facial prominences (Reid et al., 2011). Furthermore, in
643 mouse and human, cleft palate phenotypes may arise as a consequence of mutations
644 in *Wnt3* and *Wnt9b* (Niemann et al., 2004, Juriloff et al., 2006), and perturbation of
645 Wnt/β-catenin signalling has been implicated in CATSHL syndrome, a human
646 developmental disorder involving craniofacial bone malformation and mispatterning of
647 the pharyngeal arches (Sun et al., 2020). Our finding of a role for canonical Wnt
648 signalling in patterning the gill arch skeleton of skate may therefore reflect broadly
649 conserved roles for this pathway in pharyngeal skeletal development across jawed
650 vertebrates, though with the skate's possession of branchial rays offering a unique
651 anatomical readout of anterior–posterior polarity defects that arise within the
652 pharyngeal arch-derived skeleton in response to perturbations.
653
654 Our findings are also consistent with previously reported complex and context-
655 dependent roles for Wnt signalling in the regulation of cell fate determination events
656 during vertebrate skeletogenesis. In some instances, Wnt signalling functions to
657 promote skeletogenesis: for example, in chick, misexpression of *WNT5A*/*5B* promotes
658 early chondrogenesis of limb bud mesenchyme *in vitro* and delays the terminal
659 differentiation of growth plate chondrocytes *in vivo* (Church et al., 2002), and in mouse,
660 canonical WNT signalling from cranial ectoderm induces specification of osteoblast
661 progenitors of cranial dermal bone within underlying mesenchyme (Goodnough et al.,
662 2016). Conversely, in other contexts, Wnt signalling functions to inhibit chondrogenic
663 differentiation or homeostasis. In chick, signalling through WNT3, 4, 7A, 14 or FZ7
664 have all been shown to inhibit chondrogenesis *in vitro* or *in vivo* (Rudnicki and Brown,
665 1997), while in mouse conditionally-induced haploinsufficiency of the gene encoding
666 the β-catenin degradation complex component APC (i.e. activation of canonical Wnt
667 signalling) results in loss of resting zone chondrocytes and their clonal progeny in
668 developing growth plates (Hallett et al., 2021). In the limb bud, genes encoding WNT

669 ligands are expressed in the ectoderm (Kengaku et al., 1998, Parr et al., 1993,
670 Geetha-Loganathan et al., 2005), where they function synergistically with FGF
671 signalling from the apical ectoderm ridge to inhibit chondrogenesis of limb bud
672 mesenchyme and to promote soft connective tissue fates (ten Berge et al., 2008). Our
673 findings therefore demonstrate a striking parallel between developing skate gill arches
674 and tetrapod limb buds, with Wnt signals emanating from ridge-adjacent epithelia
675 functioning to inhibit chondrogenic differentiation, thereby ensuring differentiation of
676 cartilaginous appendages in a spatially-controlled manner.
677
678 We have previously shown that Shh signalling from the GAER is required for branchial
679 ray chondrogenesis in skate (Gillis and Hall, 2016), and that the application of
680 exogenous SHH protein to the anterior gill arch is sufficient to induce ectopic branchial
681 rays (Gillis et al., 2009b). However, it is unclear whether Shh from the GAER is a direct
682 inducer of chondrogenesis in the posterior arch mesenchyme, or rather induces
683 chondrogenesis indirectly, via a secondary signal (i.e. emanating from the Shh-
684 responsive epithelium or mesenchyme). We have observed that inhibition of Wnt
685 signalling in skate embryos has no effect on the expression of *Shh* in the GAER, but
686 rather results in an anterior expansion of Shh signal transduction in the gill arch
687 ectoderm, which in turn, correlates with ectopic chondrogenesis in the anterior gill
688 arch. This observation indicates that the pro-chondrogenic influence of GAER Shh
689 signalling may be indirect, occurring via a secondary Shh-depending epithelial signal
690 whose expression is typically posteriorly restricted by Wnt signalling from GAER-
691 adjacent ectoderm. The Shh and Wnt signalling pathways share multiple downstream
692 components (reviewed in; Ding and Wang (2017). For example, components of the
693 canonical Wnt signalling pathway can positively regulate Shh signalling via GSK3β,
694 by phosphorylating the downstream component SUFU and promoting the release of
695 SUFU from Gli (Takenaka et al., 2007), and by β-catenin affecting Gli1 transcriptional
696 activity via TCF/LEF (Maeda et al., 2006). It has also been found that Gli3 may function
697 as a downstream effector of the Wnt pathway, and that Wnt signalling represses Shh
698 activity in the dorsal neural tube through the regulation of *Gli3* expression (Alvarez-
699 Medina et al., 2008). Finally, the Shh signalling pathway may regulate Wnt signalling
700 through Gli1 and Gli2, with these factors positively regulating the expression of the
701 secreted Wnt inhibitor *frizzled-related protein-1* (*sFRP-1*) (He et al., 2006). These
702 mechanisms, or others, could account for the apparent cross regulation between Wnt

703 and Shh signalling that we have observed during growth and patterning of skate
704 pharyngeal arches.
705
706 Finally, conservation of *Shh*, *Fgf* and *Wnt* expression at the pharyngeal arch
707 endoderm–ectoderm boundary in skate and chick point to these as ancestral features
708 of the jawed vertebrate pharyngeal patterning programme. In bony vertebrates, the
709 PEM is a feature of the hyoid arch (Wall and Hogan, 1995). The hyoid arch of bony
710 fishes expands to form an operculum that is supported by dermal bone, and functions
711 as a protective cover for the gills that arise from the posterior pharyngeal arches
712 (Richardson et al., 2012), while the hyoid arch of amniotes expands caudally and
713 ultimately fuses with the posterior ectoderm to enclose the cervical sinus and close
714 the surface of the neck (Richardson et al., 2012). In elasmobranch cartilaginous fishes,
715 on the other hand, the GAER is a feature of the hyoid and first four gill arches, all of
716 which undergo lateral expansion to form a series of protective flaps that are supported
717 by cartilaginous branchial rays (Gillis et al., 2011). In a departure from the
718 elasmobranch condition, holocephalan cartilaginous fishes possess a GAER only on
719 their hyoid arch, and this correlates with the presence in this group of a single hyoid
720 arch-derived opercular gill cover supported by cartilaginous branchial rays, which
721 evolved convergently with the condition seen in bony fishes (Gillis et al., 2011). Recent
722 fossil data resolves the hyoid operculate condition of bony fishes as primitive for jawed
723 vertebrates (Dearden et al., 2019), with iterative lateral expansion of the gill arches
724 arising along the cartilaginous fish stem group, and with secondary loss of gill arch
725 expansion in holocephalans (Gillis et al., 2011). Therefore, while the number of
726 pharyngeal arches possessing a GAER/PEM varies across jawed vertebrate lineages,
727 the presence of these signalling centres correlates tightly with arches that undergo
728 lateral expansion, highlighting variation in GAER/PEM retention as a major
729 determinant of jawed vertebrate pharyngeal architecture. Although amniotes lack
730 homologues of the opercular series or branchial rays of bony and cartilaginous fishes,
731 respectively, further comparative work between bony and cartilaginous fishes with
732 disparate pharyngeal skeletal configurations may shed light on ancestral functions for
733 ectodermal Wnt and endodermal GAER/PEM signalling in governing pharyngeal
734 skeletal pattern and cell fate determination.
735
736

Acknowledgements

With thanks to Dr Kate Criswell and Dr Christine Hirschberger for their advice, and to the Wellcome PhD Programme in Developmental Mechanisms. The authors were funded by a Wellcome PhD studentship (214953/Z/18/Z) to JMR, and by a Royal Society University Research Fellowship (UF130182 and URF\R\191007) and Royal Society Research Grant (RG140377) to JAG.

Data Accessibility

All data and R scripts for analysis have been deposited on Figshare: 10.6084/m9.figshare.19615779

RNA sequencing data are available at NCBI-SRA under BioProject ID: PRJNA825354

Biosample accessions: SAMN27512544, SAMN27512545, SAMN27512546, SAMN27512547, SAMN27512548, SAMN27512549, SAMN27512550, SAMN27512551, SAMN27512552, SAMN27512553, SAMN27512554, SAMN27512555, SAMN27512556, SAMN27512557, SAMN27512558, SAMN27512559, SAMN27512560, SAMN27512561, SAMN27512562, SAMN27512563

Probes were purchased from Molecular Instruments (Los Angeles, California, USA). This included the following: for skate *Shh* (Lot PRA753), *Ptc2* (Lot PRA754), *Fgf8* (Lot PRA755), *Dusp6* (Lot PRA756), *Wnt2b* (Lot PRE300), *Wnt3* (Lot PRG814), *Wnt4* (Lot PRE301), *Wnt7b* (Lot PRE302), *Wnt9b* (Lot PRE303), Notum (Lot PRG817), *Kremen1* (Lot PRG816), *Axin2* (Lot PRG818), *Apcdd1* (Lot PRG815), *Col2a1* (Lot PRB574) and *Sox9* (Lot PRB571); for chick *SHH* (Lot PRB282), *FGF8* (Lot PRA997), *BMP7* (Lot PRb283), *WNT2B* (Lot PRG820), *WNT3* (Lot PRG823), *WNT4* (Lot PRG821), *WNT7B* (Lot PRG819), *WNT9B* (Lot PRG822), *NOTUM* (Lot PRG824), *KREMEN1* (Lot PRG825), *AXIN2* (Lot PRG827), *APCDD1* (Lot PRG826).

References

ALEXANDER, C., PILOTO, S., LE PABIC, P. & SCHILLING, T. F. 2014. Wnt signaling interacts with bmp and edn1 to regulate dorsal-ventral patterning and growth of the craniofacial skeleton. *PLoS Genet,* 10**,** e1004479.

ALTSCHUL, S. F., GISH, W., MILLER, W., MYERS, E. W. & LIPMAN, D. J. 1990. Basic local alignment search tool. *J Mol Biol,* 215**,** 403-10.

ALVAREZ-MEDINA, R., CAYUSO, J., OKUBO, T., TAKADA, S. & MARTI, E. 2008. Wnt canonical pathway restricts graded Shh/Gli patterning activity through the regulation of Gli3 expression. *Development,* 135**,** 237-47.

ARONESTY, E. 2011. *Command-line tools for processing biological sequencing data* [Online]. Available: https://github.com/ExpressionAnalysis/ea-utils [Accessed January 2020].

BALLARD, W. W., MELLINGER, J. & LECHENAULT, H. 1993. A series of normal stages for development of Scyliorhinus canicula, the lesser spotted dogfish (Chondrichthyes: Scyliorhinidae). *Journal of Experimental Zoology,* 267**,** 318-336.

BRITO, J. M., TEILLET, M. A. & LE DOUARIN, N. M. 2006. An early role for sonic hedgehog from foregut endoderm in jaw development: ensuring neural crest cell survival. *Proc Natl Acad Sci U S A,* 103**,** 11607-12.

CHEN, Y. 2008. *edgeR: differential analysis of sequence read count data* [Online]. Available: https://www.bioconductor.org/packages/release/bioc/vignettes/edgeR/inst/doc/edgeRUsersGuide.pdf [Accessed].

CHOE, C. P., COLLAZO, A., TRINH LE, A., PAN, L., MOENS, C. B. & CRUMP, J. G. 2013. Wnt-dependent epithelial transitions drive pharyngeal pouch formation. *Dev Cell,* 24**,** 296-309.

CHOI, H. M. T., SCHWARZKOPF, M., FORNACE, M. E., ACHARYA, A., ARTAVANIS, G., STEGMAIER, J., CUNHA, A. & PIERCE, N. A. 2018. Third-generation in situ hybridization chain reaction: multiplexed, quantitative, sensitive, versatile, robust. *Development,* 145.

CHURCH, V., NOHNO, T., LINKER, C., MARCELLE, C. & FRANCIS-WEST, P. 2002. Wnt regulation of chondrocyte differentiation. *J Cell Sci,* 115**,** 4809-18.

COULY, G., CREUZET, S., BENNACEUR, S., VINCENT, C. & LE DOUARIN, N. M. 2002. Interactions between Hox-negative cephalic neural crest cells and the foregut endoderm in patterning the facial skeleton in the vertebrate head. *Development,* 129**,** 1061-73.

COULY, G. & LE DOUARIN, N. M. 1990. Head morphogenesis in embryonic avian chimeras: evidence for a segmental pattern in the ectoderm corresponding to the neuromeres. *Development,* 108**,** 543-58.

CRISWELL, K. E. & GILLIS, J. A. 2020. Resegmentation is an ancestral feature of the gnathostome vertebral skeleton. *Elife,* 9.

DANIEL, J. F. 1934. *The elasmobranch fishes,* Berkeley,Calif., University of California press.

DEARDEN, R. P., STOCKEY, C. & BRAZEAU, M. D. 2019. The pharynx of the stem-chondrichthyan Ptomacanthus and the early evolution of the gnathostome gill skeleton. *Nat Commun,* 10**,** 2050.

DING, M. & WANG, X. 2017. Antagonism between Hedgehog and Wnt signaling pathways regulates tumorigenicity. *Oncol Lett,* 14**,** 6327-6333.

817 GEETHA-LOGANATHAN, P., NIMMAGADDA, S., ANTONI, L., FU, K., WHITING, C.
818 J., FRANCIS-WEST, P. & RICHMAN, J. M. 2009. Expression of WNT signalling
819 pathway genes during chicken craniofacial development. *Dev Dyn,* 238**,** 1150-65.
820 GEETHA-LOGANATHAN, P., NIMMAGADDA, S., PROLS, F., PATEL, K., SCAAL, M.,
821 HUANG, R. & CHRIST, B. 2005. Ectodermal Wnt-6 promotes Myf5-dependent
822 avian limb myogenesis. *Dev Biol,* 288**,** 221-33.
823 GILLIS, J. A., DAHN, R. D. & SHUBIN, N. H. 2009a. Chondrogenesis and homology of the
824 visceral skeleton in the little skate, Leucoraja erinacea (Chondrichthyes: Batoidea). *J*
825 *Morphol,* 270**,** 628-43.
826 GILLIS, J. A., DAHN, R. D. & SHUBIN, N. H. 2009b. Shared developmental mechanisms
827 pattern the vertebrate gill arch and paired fin skeletons. *Proc Natl Acad Sci U S A,*
828 106**,** 5720-4.
829 GILLIS, J. A. & HALL, B. K. 2016. A shared role for sonic hedgehog signalling in
830 patterning chondrichthyan gill arch appendages and tetrapod limbs. *Development,*
831 143**,** 1313-7.
832 GILLIS, J. A., MODRELL, M. S., NORTHCUTT, R. G., CATANIA, K. C., LUER, C. A. &
833 BAKER, C. V. 2012. Electrosensory ampullary organs are derived from lateral line
834 placodes in cartilaginous fishes. *Development,* 139**,** 3142-6.
835 GILLIS, J. A., RAWLINSON, K. A., BELL, J., LYON, W. S., BAKER, C. V. & SHUBIN,
836 N. H. 2011. Holocephalan embryos provide evidence for gill arch appendage
837 reduction and opercular evolution in cartilaginous fishes. *Proc Natl Acad Sci U S A,*
838 108**,** 1507-12.
839 GILLIS, J. A. & TIDSWELL, O. R. 2017. The Origin of Vertebrate Gills. *Curr Biol,* 27**,** 729-
840 732.
841 GOODNOUGH, L. H., DINUOSCIO, G. J. & ATIT, R. P. 2016. Twist1 contributes to
842 cranial bone initiation and dermal condensation by maintaining Wnt signaling
843 responsiveness. *Dev Dyn,* 245**,** 144-56.
844 GRAHAM, A. & SMITH, A. 2001. Patterning the pharyngeal arches. *Bioessays,* 23**,** 54-61.
845 GREVELLEC, A. & TUCKER, A. S. 2010. The pharyngeal pouches and clefts:
846 Development, evolution, structure and derivatives. *Semin Cell Dev Biol,* 21**,** 325-32.
847 HAAS, B. J., PAPANICOLAOU, A., YASSOUR, M., GRABHERR, M., BLOOD, P. D.,
848 BOWDEN, J., COUGER, M. B., ECCLES, D., LI, B., LIEBER, M., MACMANES,
849 M. D., OTT, M., ORVIS, J., POCHET, N., STROZZI, F., WEEKS, N.,
850 WESTERMAN, R., WILLIAM, T., DEWEY, C. N., HENSCHEL, R., LEDUC, R.
851 D., FRIEDMAN, N. & REGEV, A. 2013. De novo transcript sequence reconstruction
852 from RNA-seq using the Trinity platform for reference generation and analysis. *Nat*
853 *Protoc,* 8**,** 1494-512.
854 HALLETT, S. A., MATSUSHITA, Y., ONO, W., SAKAGAMI, N., MIZUHASHI, K.,
855 TOKAVANICH, N., NAGATA, M., ZHOU, A., HIRAI, T., KRONENBERG, H. M.
856 & ONO, N. 2021. Chondrocytes in the resting zone of the growth plate are maintained
857 in a Wnt-inhibitory environment. *Elife,* 10.
858 HAMBURGER, V. & HAMILTON, H. L. 1951. A series of normal stages in the
859 development of the chick embryo. *J. Morphol.,* 88**,** 49-92.
860 HE, J., SHENG, T., STELTER, A. A., LI, C., ZHANG, X., SINHA, M., LUXON, B. A. &
861 XIE, J. 2006. Suppressing Wnt signaling by the hedgehog pathway through sFRP-1. *J*
862 *Biol Chem,* 281**,** 35598-602.
863 HIRSCHBERGER, C., SLEIGHT, V. A., CRISWELL, K. E., CLARK, S. J. & GILLIS, J. A.
864 2021. Conserved and unique transcriptional features of pharyngeal arches in the skate
865 (Leucoraja erinacea) and evolution of the jaw. *Mol Biol Evol,* 38**,** 4187-4204.

866 JEZEWSKI, P. A., FANG, P. K., PAYNE-FERREIRA, T. L. & YELICK, P. C. 2008.
867 Zebrafish Wnt9b synteny and expression during first and second arch, heart, and
868 pectoral fin bud morphogenesis. *Zebrafish,* 5**,** 169-77.
869 JIANG, X., ISEKI, S., MAXSON, R. E., SUCOV, H. M. & MORRISS-KAY, G. M. 2002.
870 Tissue origins and interactions in the mammalian skull vault. *Dev Biol,* 241**,** 106-16.
871 JURILOFF, D. M., HARRIS, M. J., MCMAHON, A. P., CARROLL, T. J. & LIDRAL, A. C.
872 2006. Wnt9b is the mutated gene involved in multifactorial nonsyndromic cleft lip
873 with or without cleft palate in A/WySn mice, as confirmed by a genetic
874 complementation test. *Birth Defects Res A Clin Mol Teratol,* 76**,** 574-9.
875 KAGUE, E., GALLAGHER, M., BURKE, S., PARSONS, M., FRANZ-ODENDAAL, T. &
876 FISHER, S. 2012. Skeletogenic fate of zebrafish cranial and trunk neural crest. *PLoS*
877 *One,* 7**,** e47394.
878 KAWAKAMI, Y., RODRIGUEZ-LEON, J., KOTH, C. M., BUSCHER, D., ITOH, T.,
879 RAYA, A., NG, J. K., ESTEBAN, C. R., TAKAHASHI, S., HENRIQUE, D.,
880 SCHWARZ, M. F., ASAHARA, H. & IZPISUA BELMONTE, J. C. 2003. MKP3
881 mediates the cellular response to FGF8 signalling in the vertebrate limb. *Nat Cell*
882 *Biol,* 5**,** 513-9.
883 KENGAKU, M., CAPDEVILA, J., RODRIGUEZ-ESTEBAN, C., DE LA PENA, J.,
884 JOHNSON, R. L., IZPISUA BELMONTE, J. C. & TABIN, C. J. 1998. Distinct WNT
885 pathways regulating AER formation and dorsoventral polarity in the chick limb bud.
886 *Science,* 280**,** 1274-7.
887 KULAK, O., CHEN, H., HOLOHAN, B., WU, X., HE, H., BOREK, D., OTWINOWSKI, Z.,
888 YAMAGUCHI, K., GAROFALO, L. A., MA, Z., WRIGHT, W., CHEN, C., SHAY,
889 J. W., ZHANG, X. & LUM, L. 2015. Disruption of Wnt/beta-Catenin Signaling and
890 Telomeric Shortening Are Inextricable Consequences of Tankyrase Inhibition in
891 Human Cells. *Mol Cell Biol,* 35**,** 2425-35.
892 LANGMEAD, B., TRAPNELL, C., POP, M. & SALZBERG, S. L. 2009. Ultrafast and
893 memory-efficient alignment of short DNA sequences to the human genome. *Genome*
894 *Biol,* 10**,** R25.
895 LU, J., MA, Z., HSIEH, J. C., FAN, C. W., CHEN, B., LONGGOOD, J. C., WILLIAMS, N.
896 S., AMATRUDA, J. F., LUM, L. & CHEN, C. 2009. Structure-activity relationship
897 studies of small-molecule inhibitors of Wnt response. *Bioorg Med Chem Lett,* 19**,**
898 3825-7.
899 LUSTIG, B., JERCHOW, B., SACHS, M., WEILER, S., PIETSCH, T., KARSTEN, U.,
900 VAN DE WETERING, M., CLEVERS, H., SCHLAG, P. M., BIRCHMEIER, W. &
901 BEHRENS, J. 2002. Negative feedback loop of Wnt signaling through upregulation
902 of conductin/axin2 in colorectal and liver tumors. *Mol Cell Biol,* 22**,** 1184-93.
903 MAEDA, O., KONDO, M., FUJITA, T., USAMI, N., FUKUI, T., SHIMOKATA, K.,
904 ANDO, T., GOTO, H. & SEKIDO, Y. 2006. Enhancement of GLI1-transcriptional
905 activity by beta-catenin in human cancer cells. *Oncol Rep,* 16**,** 91-6.
906 MAO, B., WU, W., DAVIDSON, G., MARHOLD, J., LI, M., MECHLER, B. M., DELIUS,
907 H., HOPPE, D., STANNEK, P., WALTER, C., GLINKA, A. & NIEHRS, C. 2002.
908 Kremen proteins are Dickkopf receptors that regulate Wnt/beta-catenin signalling.
909 *Nature,* 417**,** 664-7.
910 MARCAIS, G. & KINGSFORD, C. 2011. A fast, lock-free approach for efficient parallel
911 counting of occurrences of k-mers. *Bioinformatics,* 27**,** 764-70.
912 MARCONI, A., HANCOCK-RONEMUS, A. & GILLIS, J. A. 2020. Adult chondrogenesis
913 and spontaneous cartilage repair in the skate, Leucoraja erinacea. *Elife,* 9.

914 MAXWELL, E. E., FROBISCH, N. B. & HEPPLESTON, A. C. 2008. Variability and
915 conservation in late chondrichthyan development: ontogeny of the winter skate
916 (Leucoraja ocellata). *Anat Rec (Hoboken),* 291**,** 1079-87.
917 NAKAMURA, T., KLOMP, J., PIERETTI, J., SCHNEIDER, I., GEHRKE, A. R. &
918 SHUBIN, N. H. 2015. Molecular mechanisms underlying the exceptional adaptations
919 of batoid fins. *Proc Natl Acad Sci U S A,* 112**,** 15940-5.
920 NIEMANN, S., ZHAO, C., PASCU, F., STAHL, U., AULEPP, U., NISWANDER, L.,
921 WEBER, J. L. & MULLER, U. 2004. Homozygous WNT3 mutation causes tetra-
922 amelia in a large consanguineous family. *Am J Hum Genet,* 74**,** 558-63.
923 NISHIMURA, O., HARA, Y. & KURAKU, S. 2017. gVolante for standardizing
924 completeness assessment of genome and transcriptome assemblies. *Bioinformatics,*
925 33**,** 3635-3637.
926 O'NEILL, P., MCCOLE, R. B. & BAKER, C. V. 2007. A molecular analysis of neurogenic
927 placode and cranial sensory ganglion development in the shark, Scyliorhinus canicula.
928 *Dev Biol,* 304**,** 156-81.
929 PARR, B. A., SHEA, M. J., VASSILEVA, G. & MCMAHON, A. P. 1993. Mouse Wnt genes
930 exhibit discrete domains of expression in the early embryonic CNS and limb buds.
931 *Development,* 119**,** 247-61.
932 PATRO, R., DUGGAL, G., LOVE, M. I., IRIZARRY, R. A. & KINGSFORD, C. 2017.
933 Salmon provides fast and bias-aware quantification of transcript expression. *Nat*
934 *Methods,* 14**,** 417-419.
935 PEARSE, R. V., 2ND, VOGAN, K. J. & TABIN, C. J. 2001. Ptc1 and Ptc2 transcripts
936 provide distinct readouts of Hedgehog signaling activity during chick embryogenesis.
937 *Dev Biol,* 239**,** 15-29.
938 PICELLI, S., FARIDANI, O. R., BJORKLUND, A. K., WINBERG, G., SAGASSER, S. &
939 SANDBERG, R. 2014. Full-length RNA-seq from single cells using Smart-seq2. *Nat*
940 *Protoc,* 9**,** 171-81.
941 REID, B. S., YANG, H., MELVIN, V. S., TAKETO, M. M. & WILLIAMS, T. 2011.
942 Ectodermal Wnt/beta-catenin signaling shapes the mouse face. *Dev Biol,* 349**,** 261-9.
943 RICHARDSON, J., SHONO, T., OKABE, M. & GRAHAM, A. 2012. The presence of an
944 embryonic opercular flap in amniotes. *Proc Biol Sci,* 279**,** 224-9.
945 ROBINSON, M. D., MCCARTHY, D. J. & SMYTH, G. K. 2010. edgeR: a Bioconductor
946 package for differential expression analysis of digital gene expression data.
947 *Bioinformatics,* 26**,** 139-40.
948 RUDNICKI, J. A. & BROWN, A. M. 1997. Inhibition of chondrogenesis by Wnt gene
949 expression in vivo and in vitro. *Dev Biol,* 185**,** 104-18.
950 SCHERZ, P. J., HARFE, B. D., MCMAHON, A. P. & TABIN, C. J. 2004. The limb bud
951 Shh-Fgf feedback loop is terminated by expansion of former ZPA cells. *Science,* 305**,**
952 396-9.
953 SHIMOMURA, Y., AGALLIU, D., VONICA, A., LURIA, V., WAJID, M., BAUMER, A.,
954 BELLI, S., PETUKHOVA, L., SCHINZEL, A., BRIVANLOU, A. H., BARRES, B.
955 A. & CHRISTIANO, A. M. 2010. APCDD1 is a novel Wnt inhibitor mutated in
956 hereditary hypotrichosis simplex. *Nature,* 464**,** 1043-7.
957 SHONE, V. & GRAHAM, A. 2014. Endodermal/ectodermal interfaces during pharyngeal
958 segmentation in vertebrates. *J Anat,* 225**,** 479-91.
959 SLEIGHT, V. A. & GILLIS, J. A. 2020. Embryonic origin and serial homology of gill arches
960 and paired fins in the skate, Leucoraja erinacea. *Elife,* 9**,** 2020.07.02.183665.
961 STREIT, A., LEE, K. J., WOO, I., ROBERTS, C., JESSELL, T. M. & STERN, C. D. 1998.
962 Chordin regulates primitive streak development and the stability of induced neural

963 cells, but is not sufficient for neural induction in the chick embryo. *Development,* 125**,**
964 507-19.
965 SUMMERHURST, K., STARK, M., SHARPE, J., DAVIDSON, D. & MURPHY, P. 2008.
966 3D representation of Wnt and Frizzled gene expression patterns in the mouse embryo
967 at embryonic day 11.5 (Ts19). *Gene Expr Patterns,* 8**,** 331-48.
968 SUN, X., ZHANG, R., CHEN, H., DU, X., CHEN, S., HUANG, J., LIU, M., XU, M., LUO,
969 F., JIN, M., SU, N., QI, H., YANG, J., TAN, Q., ZHANG, D., NI, Z., LIANG, S.,
970 ZHANG, B., CHEN, D., ZHANG, X., LUO, L., CHEN, L. & XIE, Y. 2020. Fgfr3
971 mutation disrupts chondrogenesis and bone ossification in zebrafish model mimicking
972 CATSHL syndrome partially via enhanced Wnt/beta-catenin signaling. *Theranostics,*
973 10**,** 7111-7130.
974 TAKENAKA, K., KISE, Y. & MIKI, H. 2007. GSK3beta positively regulates Hedgehog
975 signaling through Sufu in mammalian cells. *Biochem Biophys Res Commun,* 353**,**
976 501-8.
977 TEN BERGE, D., BRUGMANN, S. A., HELMS, J. A. & NUSSE, R. 2008. Wnt and FGF
978 signals interact to coordinate growth with cell fate specification during limb
979 development. *Development,* 135**,** 3247-57.
980 THIERY, A.P., STANDING, A.S., COOPER, R.L. & FRASER, G.J. 2022. An epithelial
981 signalling centre in sharks supports homology of tooht morphogenesis in vertebrates.
982 *eLife*, 11, e73173.
983 VEITCH, E., BEGBIE, J., SCHILLING, T. F., SMITH, M. M. & GRAHAM, A. 1999.
984 Pharyngeal arch patterning in the absence of neural crest. *Curr Biol,* 9**,** 1481-4.
985 WALL, N. A. & HOGAN, B. L. 1995. Expression of bone morphogenetic protein-4 (BMP-
986 4), bone morphogenetic protein-7 (BMP-7), fibroblast growth factor-8 (FGF-8) and
987 sonic hedgehog (SHH) during branchial arch development in the chick. *Mech Dev,*
988 53**,** 383-92.
989 WITTEN, P. E. & HALL, B. K. 2003. Seasonal changes in the lower jaw skeleton in male
990 Atlantic salmon (Salmo salar L.): remodelling and regression of the kype after
991 spawning. *J Anat,* 203**,** 435-50.
992 ZHANG, X., CHEONG, S. M., AMADO, N. G., REIS, A. H., MACDONALD, B. T.,
993 ZEBISCH, M., JONES, E. Y., ABREU, J. G. & HE, X. 2015. Notum is required for
994 neural and head induction via Wnt deacylation, oxidation, and inactivation. *Dev Cell,*
995 32**,** 719-30.
996
997
998
999
1000
1001
1002
1003
1004
1005
1006
1007
1008
1009
1010
1011
1012

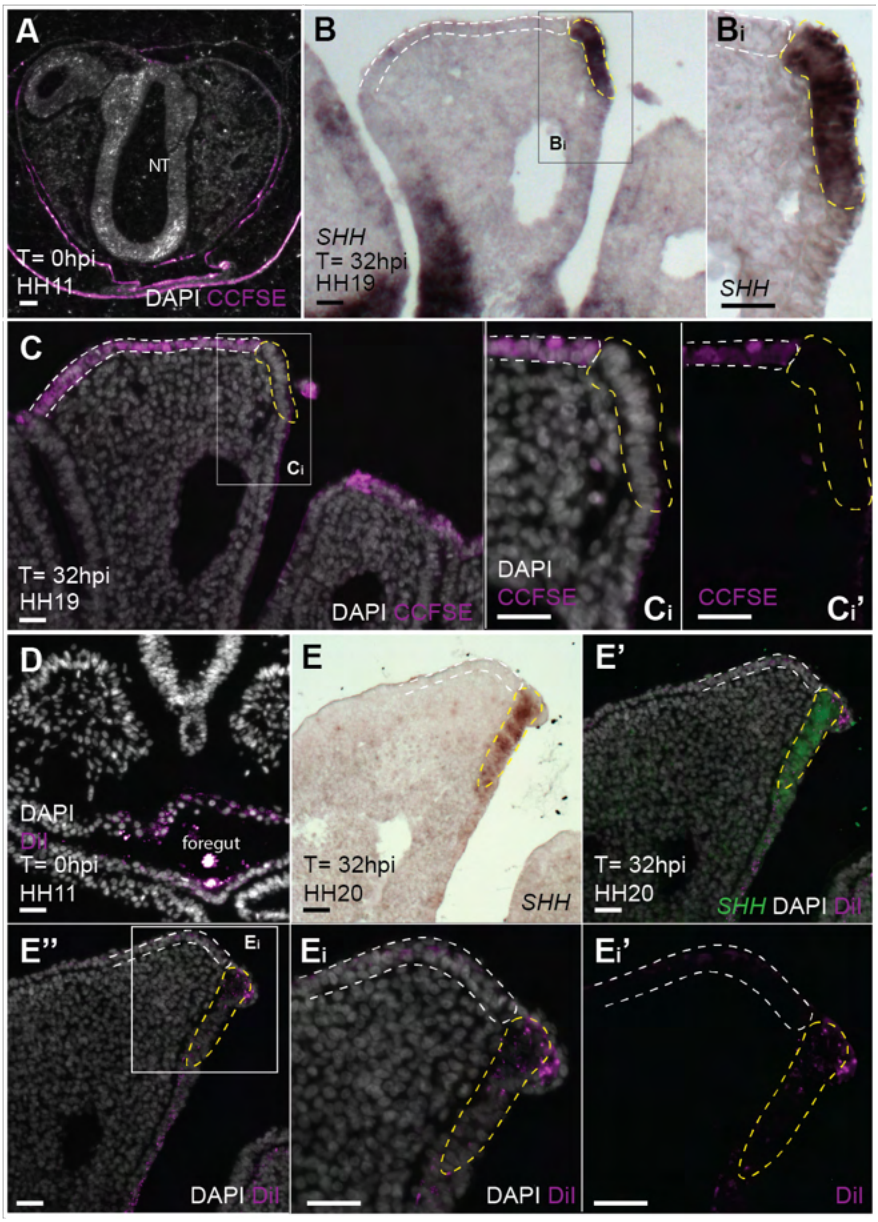

Figure 2 Supplement 1: Endodermal origin of the chick PEM. (A) Topical application of CCFSE to chick embryos at HH11 results in specific labelling of the surface ectoderm. Labelled embryos were incubated to HH19–20, by which time (**B**) *SHH* is expressed in the PEM of the hyoid arch (yellow dashed line). Imaging of CCFSE in the adjacent section from the same embryo as in **B** reveals (**C**) CCFSE-labelled hyoid arch ectoderm (white dashed line) extending up to (but excluding) the PEM**.** (**D**) Microinjection of the pharyngeal cavity with CM-DiI at HH11 results in specific labelling of the foregut endoderm. CM-DiI-labelled embryos were grown to HH19–20, at which point (**E***) SHH* is expressed in the PEM of the hyoid arch (yellow dashed line). (**E'**) Co-labelling of cells of the PEM with *SHH* and CM-DiI indicates

1024 endodermal origin of this signalling centre. A–P: Anterior–posterior axis, hpi: hours
1025 post injection, NT: neural tube. Scale bars: A = 80μm, B–E = 20 μm.
1026
1027
1028
1029
1030
1031
1032
1033
1034
1035
1036
1037
1038

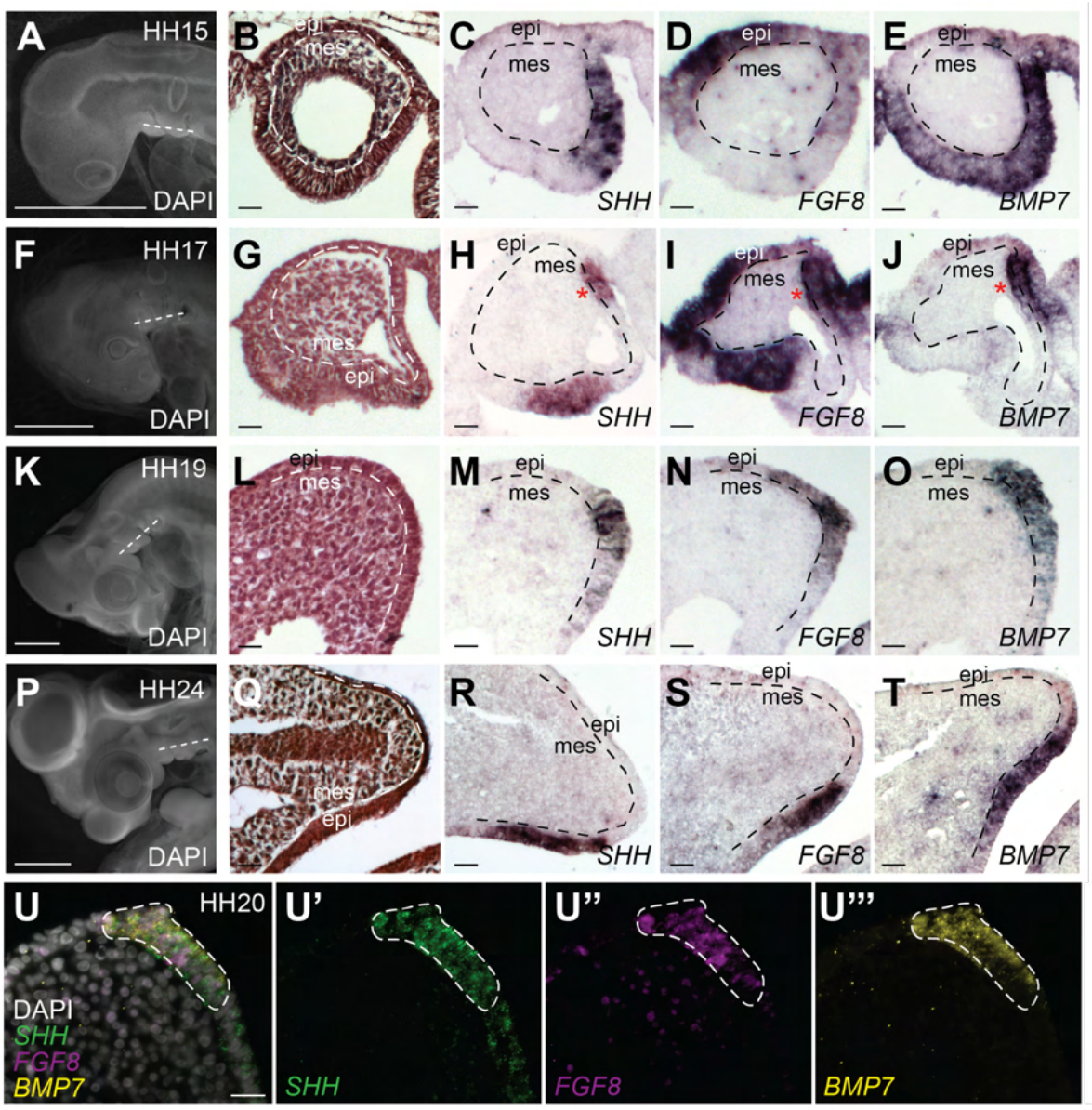

Figure 3 Supplement 1: The chick PEM co-expresses *SHH*, *FGF8* and *BMP7*. (**A**) At HH15, (**B**) endodermal pouches delineate the pharyngeal arches. (**C**) *SHH* is expressed in the posterior endodermal epithelium of the developing hyoid arch, while (**D**) *FGF8* is expressed in the lateral hyoid arch ectodermal arch epithelium and posterior endodermal epithelium, and (**E**) *BMP7* is expressed throughout the endodermal epithelium. (**F**) By HH17, (**G**) the hyoid arch begins to expand laterally, and (**H**) *SHH,* (**I**) *FGF8*, and (**J**) *BMP7* transcripts appear to be co-expressed in a domain of posterior endodermal epithelium (the presumptive PEM; indicated by red asterisk). (**K**) By HH19, (**L**) the hyoid arch is expanding caudally, and (**M**) *SHH*, (**N**) *FGF8* and (**O**) *BMP7* are co-expressed in the PEM. (**P**) By HH24, (**Q**) the hyoid arch is expanding posteriorly, lateral to the PEM and (**R**) *SHH*, (**S**) *FGF8* and (**T**) *BMP7*

1051 transcripts remain co-localised at the PEM. (**U**) ISH by HCR at HH20 shows co-
1052 expression of (**U'**) *SHH*, (**U''**) *FGF8* and (**U'''**) *BMP7* in the PEM in chick, with these
1053 three genes sharing a sharp anterior boundary. Epi: epithelial, Mes: mesenchymal.
1054 Scale bars: A,F,K,P = 2mm, all others = 20 μm.
1055
1056
1057
1058
1059
1060
1061
1062

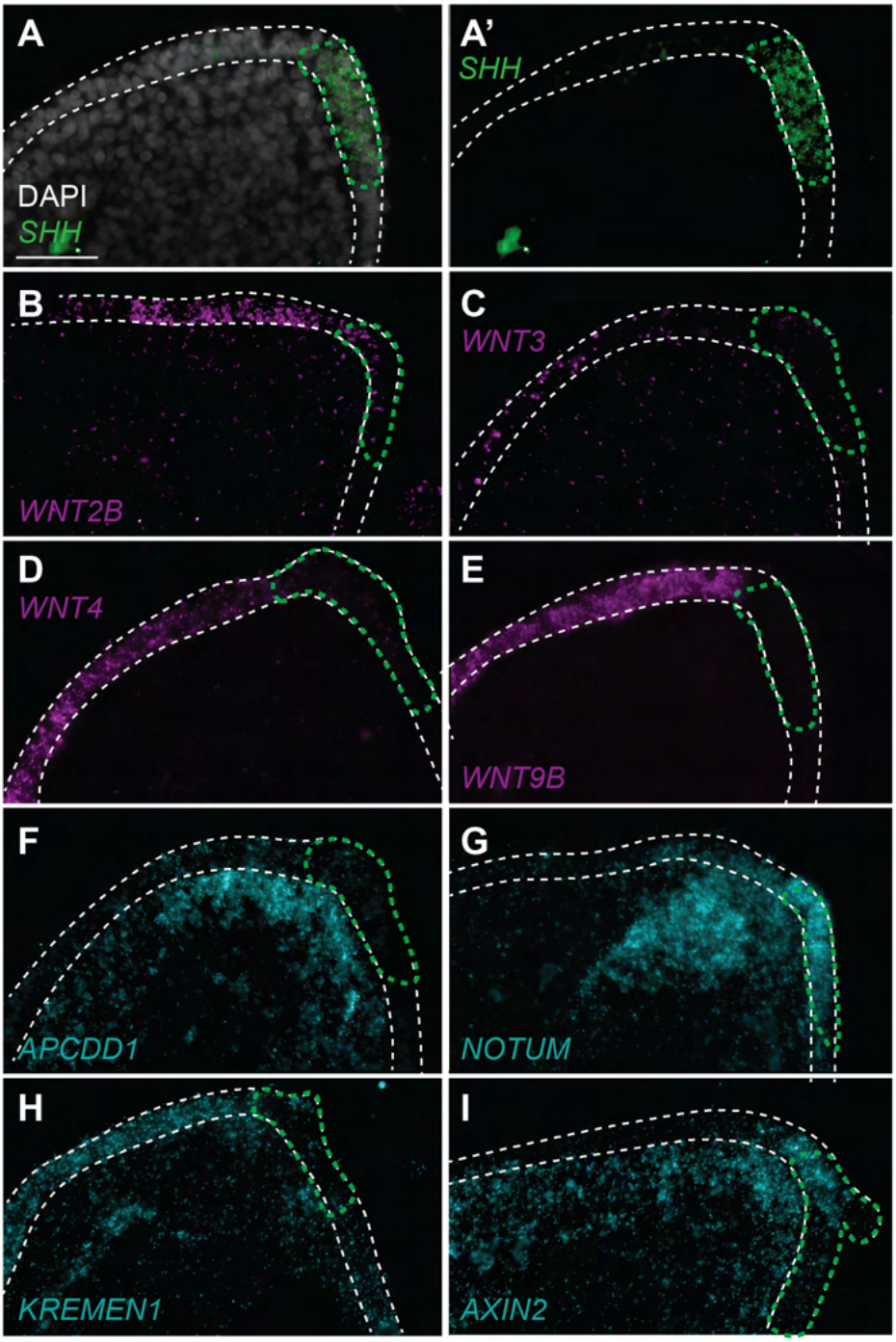

Figure 6 Supplement 1: *WNT* pathway genes are expressed in and around the PEM in chick. (**A, A'**) ISH by HCR for *SHH* was performed alongside each gene of interest as a marker of the PEM. For ease of visualisation in **B–I**, *SHH* expression is not shown but rather these PEM cells are outlined green, and the arch is outlined in white for orientation. (**B**) *WNT2B,* (**C**) *WNT3,* (**D**) *WNT4* and (**E**) *WNT9B* are expressed predominantly in the ectodermal arch epithelium adjacent to the PEM. (**F**) *APCDD1* is expressed in distal arch mesenchyme and weakly in the overlying arch epithelium. (**G**) *NOTUM* is expressed in distal arch epithelium and mesenchyme, and

1072 is expressed particularly strongly in the cells of the PEM and in the mesenchyme cells
1073 under the PEM-adjacent ectodermal epithelium. (**H**) *KREMEN1* is expressed in
1074 ectodermal epithelium adjacent to the PEM, and in distal arch mesenchyme. (**I**) *AXIN2*
1075 is expressed broadly throughout the distal arch epithelium and mesenchyme, with
1076 particularly strong expression in the anterior–distal mesenchyme and in cells of the
1077 PEM. Scale bar: 50 μm.
1078
1079
1080
1081
1082
1083
1084
1085
1086
1087

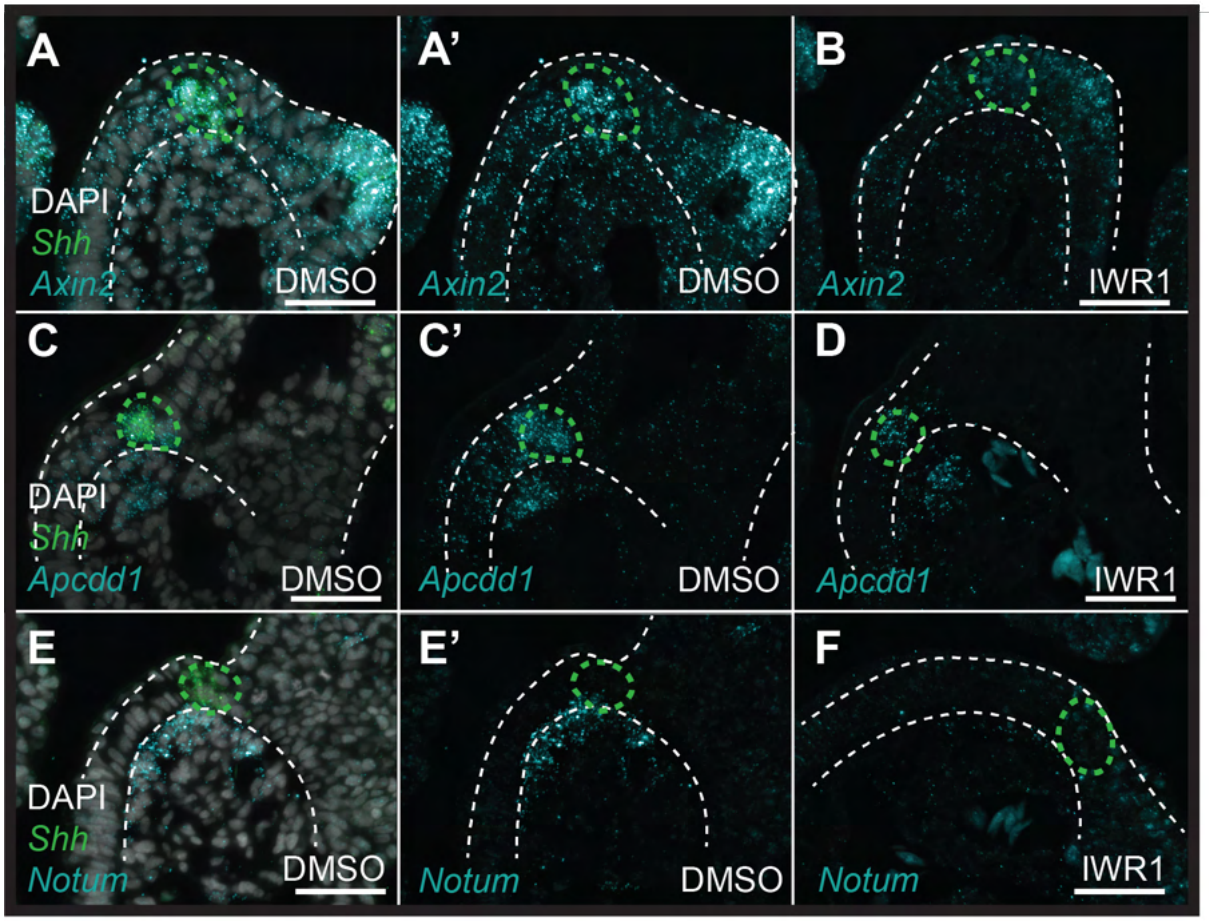

Figure 6 Supplement 2: Pharmacological inhibition of Wnt signalling in skate leads to downregulation of Wnt pathway genes. ISH by HCR was performed on sections of S26 skate embryos treated for 72hrs with either DMSO (control) or the canonical Wnt inhibitor IWR1. *Shh* was performed alongside each gene of interest as a marker of the GAER. (**A–A'**) *Axin2* is broadly expressed throughout the distal arch epithelium and mesenchyme in control embryos, with particularly strong expression in the cells of the GAER and in developing gill buds. (**B**) *Axin2* expression is substantially depressed with IWR1 treatment. (**C–C'**) *Apcdd1* is expressed in the cells of the GAER, and also within anterior–distal mesenchyme in control embryos, and (**D**) both of these expression domains show reduced expression with IWR1 treatment. (**E–E'**) *Notum* is expressed within anterior-distal arch mesenchyme in control embryos. (**F**) *Notum* expression is completely lost in the anterior-distal arch mesenchyme with IWR1 treatment. All images are representative of experiments performed in triplicate. For ease of visualisation in (**A', B, C', D, E', F**) *SHH* expression is not shown but rather these GAER cells are outlined green, and the arch is outlined in white for orientation. Scale bar: 50 μm.